Composites Part B 252 (2023) 110492

Contents lists available at ScienceDirect

Composites Part B

journal homepage: www.elsevier.com/locate/compositesb

# Development of alternative cementitious binders for 3D printing applications: A critical review of progress, advantages and challenges

Yiming Peng [a], Cise Unluer [b,*]

[a] School of Engineering, University of Glasgow, Glasgow, G12 8LT, United Kingdom
[b] Department of Mechanical, Aerospace and Civil Engineering, University of Manchester, Manchester, M13 9PL, United Kingdom

ARTICLE INFO

Handling editor: Hao Wang

*Keywords:*
3D printing
Alternative binders
Performance
Fresh properties
Mechanical properties
Applications

ABSTRACT

3D printing is a promising technology of great significance in several industries including construction. In line with the urgent need to reduce the environmental impacts of the built environment, traditional binders such as Portland cement are being substituted by suitable alternative binders. This paper systematically reviews the recent advances in the use of key alternative binders such as geopolymers/alkali-activated systems, aluminate cements, MgO-based cements, gypsum-based materials, and limestone-calcined clay-based cementitious materials in the context of 3D printing. A detailed discussion on the progress of research in the use of such alternative binders in the development of 3D-printed components is presented, highlighting the main advances made in recent years, challenges faced and potential solutions to enable the large-scale application of these products. A comprehensive evaluation of the key properties controlling the performance of 3D-printed components prepared with different mixture proportions and curing conditions is also included. The information and recommendations provided in this review aim to pave the way for the direction of future research in this area, with the goal of providing guidance on designing 3D-printed composites with the desired sustainability, cost and flexibility.

## 1. Introduction

Three-dimensional (3D) printing, also known as additive manufacturing and rapid prototyping, is a relatively new manufacturing technology based on digital models. It involves a computer-controlled system to produce a specified form of solid objects by printing and stacking an adhesive and curable material via a layer-by-layer approach [1–3]. Compared with traditional processes, the use of 3D printing presents increased accuracy and convenience by enabling the automatic manufacture of the required objects [4,5]. Furthermore, it can establish a coordination between computer software and mechanical equipment, which can effectively reduce labor consumption and improve production efficiency [6,7].

Due to these unique advantages of 3D printing technology, it has been widely used in aerospace applications [8], biomedical engineering [9], complex structure manufacturing [10], functional material molding [11] and food processing [12]. The complicated and inefficient processes (e.g. necessity to install formwork) and long periods involved in the construction of structures via traditional approaches have also led to an increased demand for the development of advanced technologies such as 3D printing to improve these aspects associated with the construction industry [13–15]. Three main molding processes used for the 3D printing of cementitious materials are contour crafting [16–18], concrete printing [19,20] and D-shape [21]. Contour crafting is a printing system that can produce objects with specific geometries through the nozzle of a gantry crane with a high printing accuracy. This technique is based on the two processes of extrusion and filling, with the first step replacing conventional formwork with 3D printing technology to produce the structural shape. Once the boundaries of each layer are established, the process of filling begins, during which the materials are poured or injected to fill the internal volume. Similar to contour crafting, concrete printing also involves the extrusion and stacking processes. However, in this approach, the structure is entirely 3D printed and hence does not need trowels, resulting in a lower printing resolution than contour crafting [22]. D-shape is a particle-bed 3D printing, during which the powder material is paved into a powder layer with a fixed thickness, and the adhesive is sprayed on the design area according to the cross-section shape to provide adhesion, followed by the paving of the subsequent powder layer [22,23]. While they present some differences in terms of their approach and intended applications, all three processes involve layered accumulative manufacturing as their core principle.

In terms of material characteristics, 3D printing can be also divided

* Corresponding author.
*E-mail address:* Cise.Unluer@manchester.ac.uk (C. Unluer).

https://doi.org/10.1016/j.compositesb.2022.110492
Received 17 May 2022; Received in revised form 10 December 2022; Accepted 23 December 2022
Available online 28 December 2022

**Acronyms**

| | |
|---|---|
| AAS | alkali-activated slag |
| BA | boric acid |
| BNS | $\beta$-naphthalene sulfonic acid type |
| CAC | calcium aluminum cement |
| CC | calcined clay |
| CF | cellulose fiber |
| CMS | sodium carboxymethyl starch |
| CSA | calcium sulfoaluminate |
| CW | ceramic waste |
| FA | fly ash |
| GGBS | ground granulated blast furnace slag |
| GW | glass waste |
| HGCC | high-grade calcined clay |
| HMCs | hydrated magnesium carbonates |
| HPMC | hydroxypropyl methylcellulose |
| $LC^3$ | limestone calcined clay cement |
| LGCC | low-grade calcined clay |
| LP | limestone powder |
| MPC | magnesium phosphate cement |
| MKPC | magnesium potassium phosphate cement |
| M/P | MgO to $KH_2PO_4$ |
| MOC | magnesium oxychloride |
| MOS | magnesium oxysulfate |
| *M-S*-H | magnesium silicate hydrate |
| NFS | naphthalene superplasticizer |
| PC | Portland cement |
| PCE | polycarboxylate superplasticizer |
| PVA | polyvinyl alcohol |
| RMC | reactive MgO cement |
| SE | starch ether |
| SF | silica fume |
| SRF | shape retention factor |
| SSA | specific surface area |
| s/b | sand-to-binder ratio |
| TA | tartaric acid |
| VMA | viscosity-modifying admixture |
| w/b ratio | water-to-binder ratio |

into extrusion-based techniques and binder jet 3D printing using powder materials and binders. Among these, extrusion-based 3D printing is more popular since the equipment used is more cost effective and can result in prototypes or replacement parts cheaply and rapidly. However, this technology has the drawback of the overhangs being only printed with the assistance of support structures, and a limited precision owing to the layered feature. In the case of binder jet, the underlying powder may be repurposed as a hanging support structure, if no printing is performed [24]. Considering the need for sufficient workability during the printing process and development of structural strength shortly after extrusion, some of the key properties of cement-based materials used in extrusion-based 3D printing are "extrudability", "flowability" and "buildability" [19,25–27]. Extrudability refers to the ability of cementitious materials to be extruded easily without blocking any of the machinery components (e.g. pipes and nozzles). Flowability is associated with the ability of a material to demonstrate a smooth and continuous flowing process that enables a high efficiency during 3D printing, resulting in an easy flow without any segregation or bleeding. During 3D printing, flowability usually refers to the "deliverability" or "pumpability" of the cementitious mix in the pipe. Finally, buildability is used to explain the ability of a material to achieve shape compliance during extrusion and layer-by-layer stacking, without any deformation or collapse under the stress generated by subsequently deposited layers.

While these aspects provide a useful guidance in the development of mixes for 3D printing applications, they need to be quantitatively verified. Considering that the extrusion process of cementitious materials from nozzle to hardening involves a dynamic flow and deformation process, the workability of these materials can be characterized by rheological parameters [28–31]. In line with their definitions, extrudability corresponds to the static rheology and thixotropy of cementitious materials and is closely related to the static yield stress (i.e. the minimum stress required to initiate flow in a paste, which is linked with the state of the microstructure that forms via colloidal flocculation and bonding provided by cement hydrate phases that can handle some stress before breaking down) [32–37]. Alternatively, flowability corresponds to the dynamic rheology [25], whereas buildability is related to the structural build-up [38,39] (Fig. 1). In addition to these properties, the mechanical performance of the multi-layer printed component, traditionally assessed by the measurement of compressive and flexural strength as well as the interlayer bond strength, needs to be evaluated to determine the success of the 3D printing process [40,41].

Regardless of the type of process used, 3D printing entails the development of cementitious binders that can satisfy these requirements in fresh and hardened states. Amongst the components of concrete mixes (e.g. binder, coarse and fine aggregates, water and various chemical or mineral admixtures), binder and water are the main ones that affect the workability, mechanical properties, volume stability (plastic shrinkage) and durability of the mix and final structure [26,42]. At present, Portland cement (PC) is the most widely used binder worldwide [43,44]. However, the mass production and application of PC lead to the emission of high concentrations of greenhouse gases that contribute to climate change [45]. Considering that approximately 4.1 billion metric tons of cement are globally produced every year, accounting for 8%–10% of the global anthropogenic carbon dioxide emissions [46–49], the production of PC is expected to become the third largest carbon emission source after fossil fuels and land-use change (e.g. deforestation) [50,51].

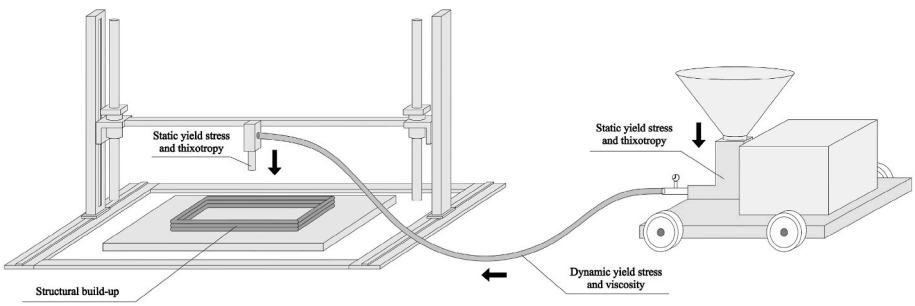


**Fig. 1.** Simplified 3D printing process and corresponding properties of extrusion-based materials (the main structure of 3D printer is based on [36]).

Furthermore, PC production requires a significant amount of natural resources, damages the ecological environment, hinders the sustainable development of social economy and consumes an average of 10–11 EJ of energy per year, accounting for 2–3% of global energy consumption [52].

These concerns associated with the production and use of PC led to the development of alternative binders with lower $CO_2$ emissions and energy consumption [53,54]. These initiatives involve the partial or complete replacement of PC in specific applications, thereby reducing the environmental impact of concrete structures [55]. Some of the most promising alternative binders developed include geopolymers and alkali-activated materials [56–58], aluminate cements [59,60], magnesia (MgO)-based cements [61–63], gypsum-based materials [64,65], and limestone-calcined clay-based cementitious materials [66–68]. Taking two of these alternative cementitious materials (i.e. alkali-activated materials and reactive MgO-based cements) as an example, depending on their chemical composition and production conditions, these binders can potentially produce formulations with lower carbon footprints than PC. In the case of MgO-based cements, the decomposition of magnesite releases a greater amount of $CO_2$ than that of limestone (1.1 vs. 0.78–0.83 t/t), resulting in a higher climate change score for MgO, despite the lower calcination temperatures [69]. However, when the carbonation potential of MgO-based cements is taken into account, their net $CO_2$ emissions can be >70% lower than PC. Alternatively, the Global Warming Potential (GWP) index corresponding to 1 $m^3$ of alkali-activated binary concrete was reported as 210.9 kg·$CO_2$·eq, which is ~45% lower than that of PC, indicating the potential for reduced environmental impacts with the use of these binders, depending on the factors mentioned above [70]. In line with the variations in their chemical formulations, each binder presents different advantages from a performance and sustainability standpoint, covering a range of applications.

One promising application for alternative binders involves the development of sustainable 3D printed components that could be used in various applications within the construction industry. These range from precast and containment elements to reinforcement for sealing elements, as well as reinforcements incorporating various materials (e.g. steel or fibers) [71]. Considering the role these binders can play in reducing the pressure on the environment caused by cement production and use, it is critical to understand their potential to be incorporated in new advances in the construction sector and determine their synergy with other innovative technologies.

A summary of the main framework presented in this paper is shown in Fig. 2. Aiming to provide a comprehensive guideline for different users including researchers, construction industry practitioners, policy makers, public members and communities working or interested in this area, this paper presents a detailed discussion on the progress of research in the use of these alternative binders in 3D printed components. The discussion also highlights the main advances made in recent years, the challenges faced and potential solutions to enable the large-scale application of these products. A comprehensive evaluation of the key properties controlling the performance of 3D components involving alternative binders prepared with different mixture proportions and curing conditions is also included. A comparison of each binder system in terms of their advantages and shortcomings associated with 3D printing is presented, underlining the long- and short-term prospects of these alternatives in automated construction. Finally, a series of recommendations are provided to pave the way for the direction of future research in this area, with the goal of providing guidance on designing 3D-printed composites with the desired sustainability, cost and flexibility aspects.

## 2. Geopolymers/alkali-activated systems

Alkali-activated binders involve materials with pozzolanic activity and alkaline activators. Alkali-activated systems enable the recycling of industrial wastes, while also reducing energy consumption and environmental pollution, depending on their composition [72,73]. Concrete made of alkali-activated binders could be more resistant to chloride ion and acid corrosion than PC due to the properties of the hydration products [74,75]. Furthermore, since the network structures in these systems are similar to that of organic thermoset polymers, they are also commonly referred to as “inorganic polymers” or “geopolymers” [76].

Geopolymers are three-dimensional network-structured aluminosilicate cementitious materials composed of $SiO_4$ and $AlO_4$ tetrahedral units formed by combining calcined minerals (e.g. metakaolin) or industrial wastes (e.g. fly ash, FA, and ground granulated blast furnace slag, GGBS) with alkali activators [77–79]. The formation of geopolymers involves three stages: (i) Si, Al monomer dissolution, (ii) monomer reconstruction and (iii) polycondensation [80–82]. The aluminosilicate precursors of geopolymers can also be classified into three categories based on the Ca content of the raw materials: Non calcium (e.g. metakaolin), low calcium (e.g. Class F FA) and high calcium (e.g. GGBS). Geopolymers have also been used in 3D printing applications as an environmentally-friendly alternative binder to reduce waste creation and PC utilization [83,84]. The following section outlines the research progress in the use of alkali activated systems/geopolymer mixes in 3D printing.

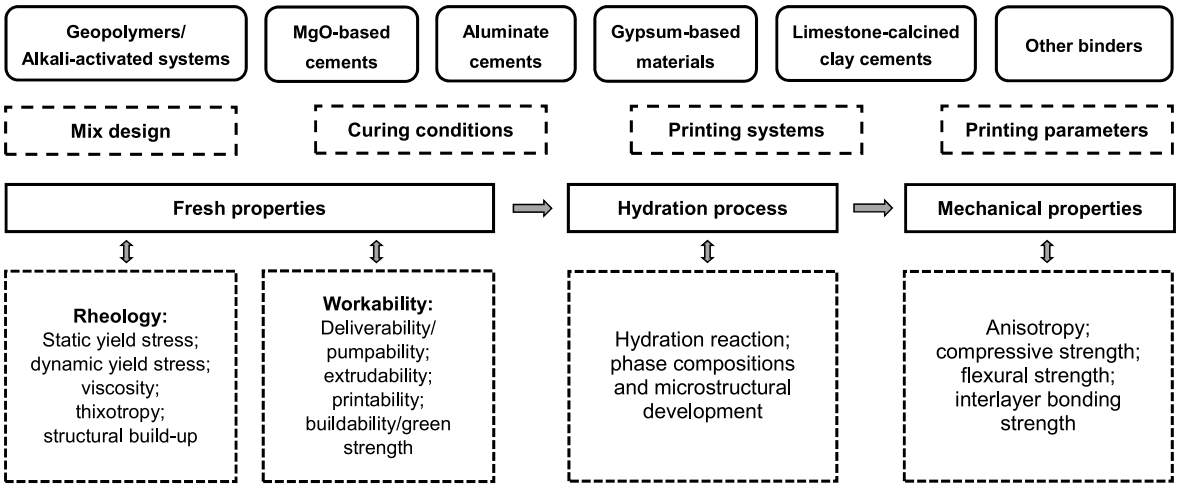


**Fig. 2.** Comprehensive framework presented in this study.

### 2.1. Rheology

Rheology has a significant impact on the early performance of 3D printed alkali-activated systems/geopolymers. A consistent development of microstructure build-up and yield stress with time is key for keeping the mixture stable throughout the entire 3D printing process from extrusion to hardening [85]. Previous studies [86] explored the role of sand-to-binder ratio (s/b) on the rheological characteristics of FA-GGBS-silica fume (SF) geopolymer mortars by varying the mixture proportions. It was reported that the yield stress of mortar rose substantially with the s/b ratio. When the s/b ratio increased to 1.7, excessive yield stress caused poor mortar extrusion and, as a result, nozzle blockage. In another study [87], the influence of activator solution molar ratio, water-to-solid ratio, activator solution-to-binder ratio and nanoclay addition on the yield stress and viscosity of geopolymer mortars were investigated. The yield stress and viscosity dropped significantly when the water-to-solid ratio and solution-to-binder ratio were increased.

Alternatively, higher molar ratio and nanoclay contents enhanced both the yield stress and viscosity. When an alkaline activator (i.e. sodium hydroxide) was employed to replace water in an equivalent mass ratio, the yield stress of the fresh paste reduced while the cohesiveness increased [88]. Higher Si/Na ratios in the alkali activator corresponded to lower viscosity and yield stress in geopolymer mixes [85]. Ishwarya et al. [89] investigated the rheological properties of FA-GGBS geopolymer mixes containing $Na_2CO_3$/$Na_2SiO_3$ as an activating solution, and revealed that the yield stress of composite pastes incorporating 25 wt% GGBS was considerably higher than those only containing FA. Increases in GGBS content could significantly improve the compressive strength of hardened pastes, which provided an experimental basis for improving the structural build-up and mechanical strength of 3D printed geopolymer mixes. However, in a different study, the substitution of GGBS with FA or SF was shown to increase the static yield stress, structural build-up rate, and thixotropy of the original alkali-activated slag (AAS) system deposited within 30 min [90]. The addition of 10 wt% SF significantly increased the viscosity in the recovery stage and thixotropy recovery rate of these mortars [91]. Considering that thixotropic recovery rate is a crucial characteristic influencing the shape retention of fresh 3D printed structures, the inclusion of SF plays a key role in improving the thixotropic properties of geopolymer mixtures. Furthermore, the use of high GGBS contents (90 wt%) was demonstrated to significantly improve the structural recovery rate of FA-based alkali-activated pastes [90]. This modification can be attributed to factors including the coupled flocculation-dissolution-reaction process of alkali-activated materials and the morphological properties of precursors.

In addition to the initial mix composition, various admixtures can also affect the rheological properties of geopolymer mixes. The fresh properties of AAS can be adjusted by adding nucleation seeds and nanoclay [92]. Due to the absorption of silicate anions on the slag surface, which results in large double-layer repulsive forces, the yield stress of AAS mixes is relatively low. However, the yield stress can more than triple after the incorporation of 0.4 wt% nanoclay, which can result in rapid flocculation, enabling the mix to reach the optimal thixotropy range for 3D printing. Sun et al. [93] prepared a geopolymer mix with GGBS, calcium carbonate powder (i.e. used as an inexpensive and inert coarse aggregate), and different contents of sodium carboxymethyl starch (CMS) as a modifying admixture. When the CMS content ranged between 4% and 6%, the corresponding plastic viscosity and yield stress were 10.08–10.42 Pa s and 32.53–66.71 Pa, respectively. These values corresponded to an ideal range that enabled a continuous printing process without any deformation after extrusion.

### 2.2. 3D printing performance

#### 2.2.1. Early-age performance

Optimizing the performance of cementitious materials at an early stage is a key issue that needs to be addressed when implementing 3D printing. The workability required in the printing process primarily includes structural integrity, uniformity, and dimensional accuracy of the printed samples, which can be evaluated via visual inspection, as well as some parameters that can be measured experimentally such as open time (i.e. the time interval between the addition of alkaline activator and the mixture exhibiting poor extrudability) and shape retention ability [87,94].

In terms of workability, concrete designed for 3D printing should have adequate self-compacting properties, but not a significant slump flow. The designed mixes must be able to retain their original shapes while the upper layers are gradually deposited over the printed lower layers [95]. Fig. 3(a)-(c) present 3D printed geopolymer monolayer samples deposited at a constant (90 mm/s) and varying speeds, as well as a multi-layered structure printed at a constant speed [96]. By comparing the bead and nozzle widths of the lines printed at different speeds (Fig. 3(b)), it was found that the width of the sample printed at 90 mm/s was the same as that of the nozzle. Therefore, this speed was used to print a multi-layered structure (Fig. 3(c)), which maintained its shape and integrity after extrusion without any collapse associated with upper layer stress or uneven extrusion. Bong et al. [94] used a 15 × 30 mm nozzle to evaluate the extrudability of FA-GGBS geopolymer mortars, and showed that there was no clogging phenomena in any of the mix proportions and the specimens generated by the 3D printer exhibited good uniformity. Furthermore, geopolymer mixes incorporating K-based activators demonstrated higher yield stress and better shape retention ability than those containing Na-based activators in general [97]. Panda et al. [91] studied the influence of thixotropic parameters (i.e. structural recovery level) on the shape retention factor (SRF) of geopolymer mortars. As shown in Figs. 4 and 5, the recovery rate of 100 wt% FA mix and its corresponding SRF were both minor, indicating that the shape retention ability of the mortar after extrusion from the nozzle was rather poor.

Although the buildability of alkali-activated materials for 3D printing is assessed to ensure that their shape remains consistent with the original design after extrusion, the early setting and rapid hardening characteristics of alkali activated materials [98], particularly after the precursors are completely mixed with alkaline activator, may result in rapid pipeline blockage during pumping. Therefore, in addition to thoroughly blending all the constituents before the printing process, one approach may involve the introduction of the alkaline activator near the print head and mixing with other components right before the extraction process. Throughout this approach, the slurry can remain inactive during transportation, significantly extending the effective pumping time, thereby improving extrudability and potentially buildability.

#### 2.2.2. Mechanical performance

From the perspective of mix design, modifiers and other additives of various types and dosages can have an impact on the mechanical performance of 3D printed geopolymer mixes. After the addition of 1% nano graphite platelets, the compressive and flexible strengths of 3D printed FA-GGBS-SF specimens were reported to increase by 28% and 89%, respectively, [99]. However, the 28-day compressive strength of GGBS-$CaCO_3$ geopolymer pastes reduced from 84.37 to 55.80 MPa and the flexural strength reduced from 12.73 to 8.17 MPa as the CMS content increased from 0% to 8% [93]. These reductions in mechanical performance were associated with an increase in porosity and a decrease in reaction rate between the GGBS powder and alkaline activator, induced by the inclusion of CMS. Differences in the anisotropic mechanical properties of alkali-activated materials, another important characteristic of 3D-printed structures, were shown to diminish with time due to the progressive production of hydration reaction products [100].

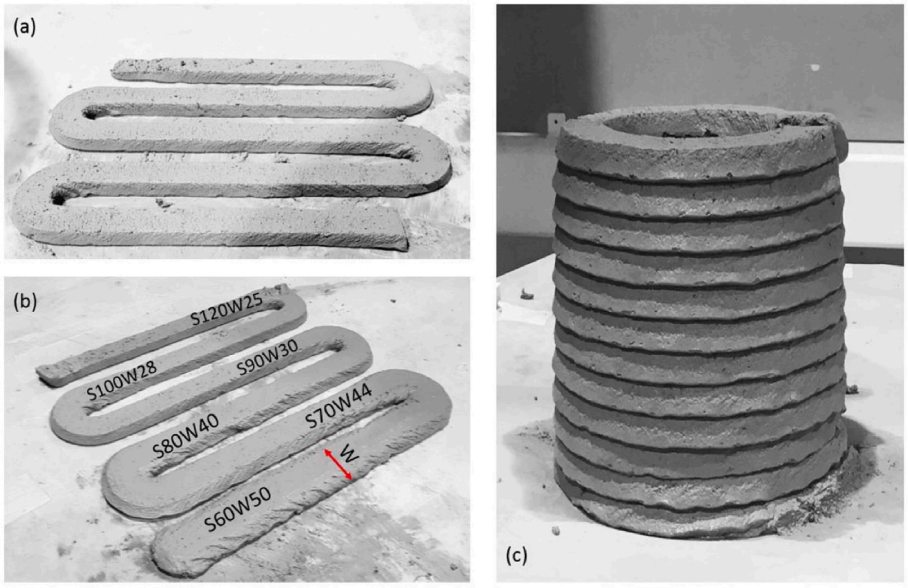


**Fig. 3.** Images of 3D printed FA-GGBS geopolymer mixes, showing: (a) Samples printed at a constant speed (90 mm/s), (b) samples printed at different speeds, and (c) printed structure composed of several layers (reproduced from Ref. [96]).

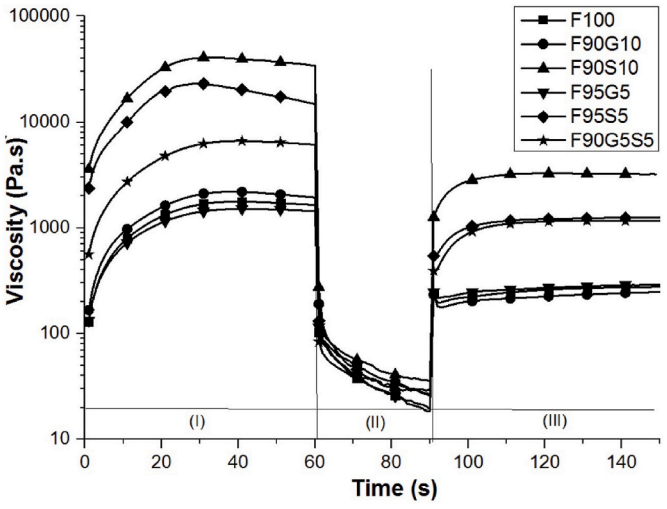


**Fig. 4.** Viscosity recovery rate of geopolymer blends incorporating different contents of FA, GGBS and SF (reproduced from Ref. [91]).

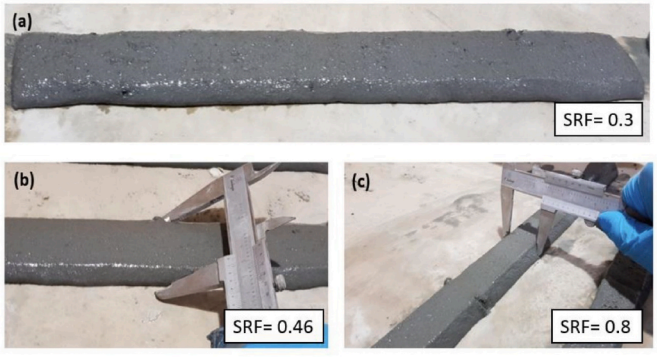


**Fig. 5.** Shape retention factors of extruded filament width with different mix designs: (a) F100 (b) F90G10, and (c) F90S10 (reproduced from Ref. [91]).

Furthermore, low activation reactivity and strong thixotropy aggravate anisotropy as a consequence of high content FA incorporation.

One-part geopolymers consisting of an aluminosilicate precursor and solid alkaline activator have been widely investigated [101]. The compressive strength of one-part FA-GGBS geopolymer samples can be significantly increased with GGBS content due to the formation of *C*–S–H and potassium alumino-silicate hydrate (K-A-*S*-H) gels [96]. The minimum GGBS content required for the preparation of FA-GGBS geopolymers via a powder-based 3D concrete printing technology was 50%, with a corresponding 7 d compressive strength of 25 MPa [102]. In terms of activators, mechanical performance can be further improved by adjusting the $SiO_2/Na_2O$ molar ratio of sodium silicate solution and the concentration of NaOH solution.

Due to their high tensile strength and elongated structure, fibers can restrict the further development of concrete fractures and substantially enhance bending strength, elongation, and toughness. The shift in the failure mode of a micro-cable reinforced composite structure from brittle to ductile with multiple cracks indicates that incorporation of this reinforcement changes the strain evolution mode when compared with non-reinforced structures, leading to improved bending and load capacity [103]. Lim et al. [104] explored the influence of polyvinyl alcohol (PVA) fibers and stainless steel cable on the bending strength of FA-based geopolymer mixes. The main failure modes of geopolymer samples were in the form of compression crushing at the top layer, with a small number of samples experiencing shear slipping between the interlayer bonds, as illustrated in Fig. 6(a) and (b). As the load increases in the four-point bending test, the sample develops a series of bending cracks that extend upward through the printed layers. The steel cable takes the majority of the load when the concrete breaks in the geopolymer specimens strengthened with hybrid reinforcement, while the PVA fibers at the crack tip offer a minor amount of tensile strength. When compared, hybrid reinforced geopolymer samples outperform the control sample (i.e. without fiber) in terms of flexible strength. Despite the evidence that micro-cables and geopolymer mixes have significant coordination and bonding effects, cable has varied impacts on the cement matrix under compressive, shear and tensile loading conditions [105,106]. Under compression, the restraint effect of micro-cables is the basis of ductility and toughness. Shear strength mainly depends on the weak plane direction of the binder between tow filaments, while tensile strength is determined by micro-cable reinforcements and the

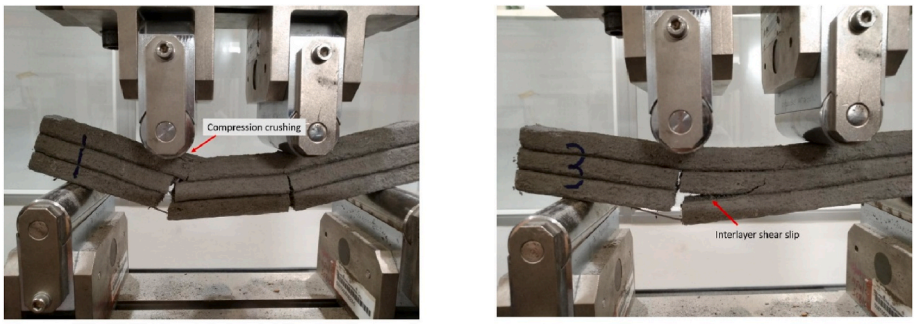


(a) Compression crushing at top layer of printed geopolymer

(b) Shear slip between printed geopolymer filaments

**Fig. 6.** Two destruction forms of 3D printed geopolymer during 4-point bending test, showing: (a) compression crushing and (b) shear slip (reproduced from Ref. [104]).

configurations. Previous studies [107] showed that specimens with flax fibers performed better than those with carbon fibers in terms of mechanical performance.

Good interlayer bond strength is also a key parameter to ensure the integrity of 3D printed cementitious materials. Previous studies [108] showed that in addition to the properties of the geopolymer itself, printing parameters also affect the bond strength of geopolymer mixes. While a large time gap between layers decreases the bond strength, smaller nozzle standoff distance and printing speed correspond to higher bond strength. Considering that the interface between layers can be uneven after incorporating certain types of fiber, the addition of fibers such as steel fibers into 3D printed geopolymer-based concrete may hinder the adhesion of subsequent layers [109]. In contrast, another study [110] revealed that the inclusion of steel fiber did not weaken the binding strength between printed layers, despite the fact that the steel fibers did not seem to bridge the interlayer surfaces. The impact and mechanism of steel fibers on the characteristics of 3D-printed geopolymers still need to be further investigated.

### 2.3. Microstructure

Fig. 7 shows the SEM images of 3D printed geopolymer mixes at different locations. Fig. 7(a) was taken from the middle area of the bottom layer, where Fig. 7(b) was taken from the interlayer area [111]. By comparing the micro-morphologies of the two locations, it can be observed that the pores in Fig. 7(a) were small and the hydration

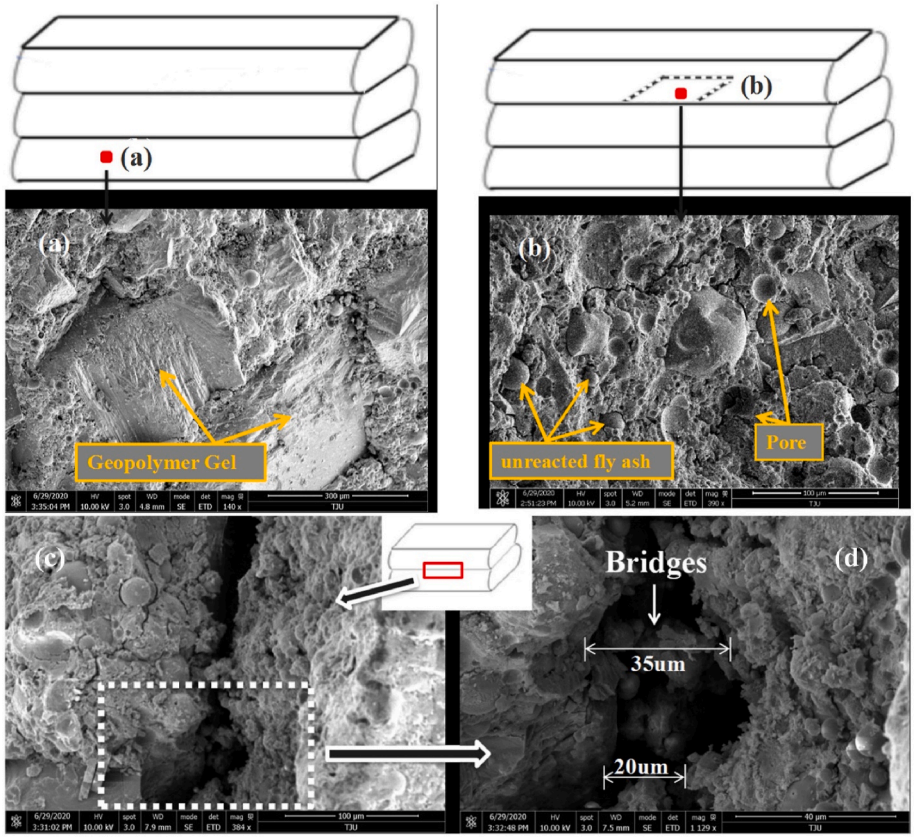


**Fig. 7.** SEM images of samples with 80%FA, 10%GGBS and 10% SF, showing: (a) middle section and (b), (c) and (d) interlaminar section (reproduced from Ref. [111]).

product (geopolymer gel) was densely distributed, whereas a larger number of pores and unreacted FA particles can be seen in Fig. 7(b). At a higher magnification shown in Fig. 7(b), a 20–35 μm crack was found between the two interfaces, where the bond strength between the cracks was generated by the bridge connection. SEM analysis revealed that the center of 3D printing blocks was more compact than the surface inter-laminar due to a superior geopolymer gel formation, showing that the interlayer bonding was relatively weak.

## 3. MgO-based cements

MgO cement is considered as a promising cementitious material, where MgO is used as the main binder to replace traditional PC. Some of the main advantages of MgO include its low $CO_2$ emissions associated with the lower temperatures and alternative sources used during its production [69]. The precursor can be magnesium carbonate ($MgCO_3$) or other materials such as $Mg(OH)_2$, sea water or brine [69,112,113]. The final product, MgO, can be divided into four grades according to the calcination temperature used during the conversion of $MgCO_3$ into MgO: (i) light-burned (reactive), (ii) hard-burned, (iii) dead-burned and (iv) fused [114,115]. The reactivity, crystal size and structure, pore structure and specific surface area (SSA) of MgO produced at different calcination temperatures vary, resulting in different uses for each grade. Among these, the calcination temperature of light-burned MgO is 700–1000 °C, which translates in a high SSA and reactivity, enabling this product to be used as a binder in various concrete mixes [61,116,117]. Compared with light-burned MgO, hard-burned MgO has a lower reactivity and slower hydration rate, therefore it is typically used as an expansive agent [118,119]. Dead-burned and fused MgO are hardly reactive, mainly used in the refractories industry [120].

### 3.1. Reactive MgO-based cements

Reactive MgO cement (RMC) formulations were initially developed by mixing different proportions of RMC and PC [121]. In the absence of any admixtures, the hydration mechanism of MgO simply involves its reaction with water to form magnesium hydroxide ($Mg(OH)_2$). The above reaction can be divided into three stages: (i) Contact of water with the surface and its gradual entry into the internal structure through the pores of MgO particles; (ii) dissolution of MgO in the presence of water, and the change in its porosity and surface composition; and (iii) formation of supersaturated $Mg(OH)_2$ on the surface of MgO particles, which can hinder the continuation of the hydration process [61,122]. Therefore, it is necessary to improve the hydration rate of MgO to result in a more compact microstructure enabled by the increased formation of reaction products that will lead to enhanced mechanical properties within the hardened mixes. Some of the main cementitious systems, in which RMC is used as the main binder include carbonated RMC mixes that may also incorporate PC and SCMs; and magnesium silicate cement systems. The following sections outline the research progress on the use of these binders in 3D printing applications.

#### 3.1.1. Carbonated RMC systems

Since the hydration of RMC is not sufficient for the development of a high mechanical performance, the use of accelerated carbonation as a part of the curing process has been extensively studied. As a part of this initiative, samples were subjected to increased concentrations of $CO_2$ (i.e. usually ranging between 5 and 20% [123], along with some studies using 100% [124]), which accelerated the reaction of $Mg(OH)_2$ with $CO_2$ to form hydrated magnesium carbonates (HMCs), the main sources of strength in RMC mixes [123,125]. This also highlighted that carbonated RMC systems could provide a solution for the permanent sequestration of $CO_2$ in the form of carbonate phases [126,127], defining this system as a potentially promising alternative binder from a sustainability perspective [69,128].

A recent study [25] looked into the 3D printing performance of RMC mortars containing 54% RMC, along with other additives such as 3% caustic MgO (with a purity of >98%), magnesium acetate (the primary liquid media), superplasticizer (polycarboxylate ether), defoamer (non-ionic surfactant) and suspension aid additive (hydroxyethyl-cellulose). Results showed that the 3D printed samples differed from the cast versions in terms of their mechanical properties, phase composition and microstructure. Similar to *P*C-based mixes, challenges were present in formulating a binder composition with a good workability only by mixing RMC and $H_2O$. Therefore, 3 wt% caustic MgO was added to accelerate the early hydration of the initial system, thereby enabling the layer-by-layer stacking process. These initiatives clearly highlighted the importance of mix design in producing structures that could maintain their integrity and uniformity without any obvious cracks or layer detachment during and after the 3D printing process.

Even in the absence of any hydration enhancing additives, the hydration rate of RMC is generally higher than that of PC in the early stages (first 10 h). For the rheological measurements (shear stress *vs.* shear rate), RMC systems demonstrate a sharply increasing curve at low shear rates, followed by a rapid decline in the rheological curve. The shear stress reaches a maximum (1.98 kPa) at a shear rate of 0.42 $s^{-1}$. When the shear rate is in the range of 10 $s^{-1}$ and 100 $s^{-1}$, the relationship between shear stress and shear rate approximately follows the "Bingham model", resulting in a yield stress of 0.95 kPa [25]. A comparison of the rheological parameters presented in earlier studies [25,129–131] revealed that RMC systems demonstrated much higher yield stress, plastic viscosity, and yield stress growth rate with time (structural build-up rate) than PC systems. These outcomes indicated that although the fluidity of RMC was lower than that of PC in the early stages, the faster structural build-up rate of RMC was beneficial in maintaining a good shape compliance during the 3D printing process.

In terms of the mechanical properties and microstructure of the hardened mixes, 3D printed RMC mortars were reported to have larger compressive strengths than those obtained by casting, which were also associated with the increased carbonation rate in line with the higher initial porosity of the printed samples [25]. Within mixes that contain larger and better-connected pores, a higher amount of $CO_2$ can diffuse into the matrix through the pores, increasing the rate and degree of the carbonation reaction, as well as enhancing the compressive strength. Fig. 8 shows a comparison of the microstructure of the cast and 3D printed RMC samples. The surface of cast samples was mainly composed of loose and large flakey dypingite, while the main products observed in the interior section was uncarbonated brucite, along with the formation of larger dypingite crystals. In contrast, the microstructural images of the 3D printed samples showed that the surface was mainly composed of small and densely distributed hydromagnesite, while the interior consisted of both hydromagnesite and dypingite.

#### 3.1.2. RMC-$SiO_2$ systems

Another typical RMC-based cementitious system is magnesium silicate cements, which are obtained by combining RMC with a $SiO_2$ source to form magnesium silicate hydrate (*M-S-*H) [132,133]. The use of various silicate-rich wastes such as SF [134], rice husk ash [135], ceramic waste (CW) and glass waste (GW) [136] as raw materials has been explored in this system. *M-S-*H can achieve 28-day compressive strengths of up to 65 MPa under ambient curing conditions (i.e. without the need for any additional accelerated $CO_2$ curing) [137]. The physicochemical properties of *M-S-*H are determined by precursors types and characteristics, mix design and curing conditions [138–140].

Relying on the rapid hydration rate of RMC in the early stages and high strength provided by the formation of *M-S-*H, previous studies [141] studied the use of RMC-$SiO_2$ mixes in 3D printing. By adjusting the mass ratio of RMC and microsilica, w/b ratio and superplasticizer content, RMC-$SiO_2$ pastes achieved an appropriate fluidity, with a recovery of up to 80% of the initial viscosity within 60 s. These properties highlighted the extrudability of RMC-$SiO_2$ mixes and their ability to return to their original workability shortly after being extruded from the nozzle.

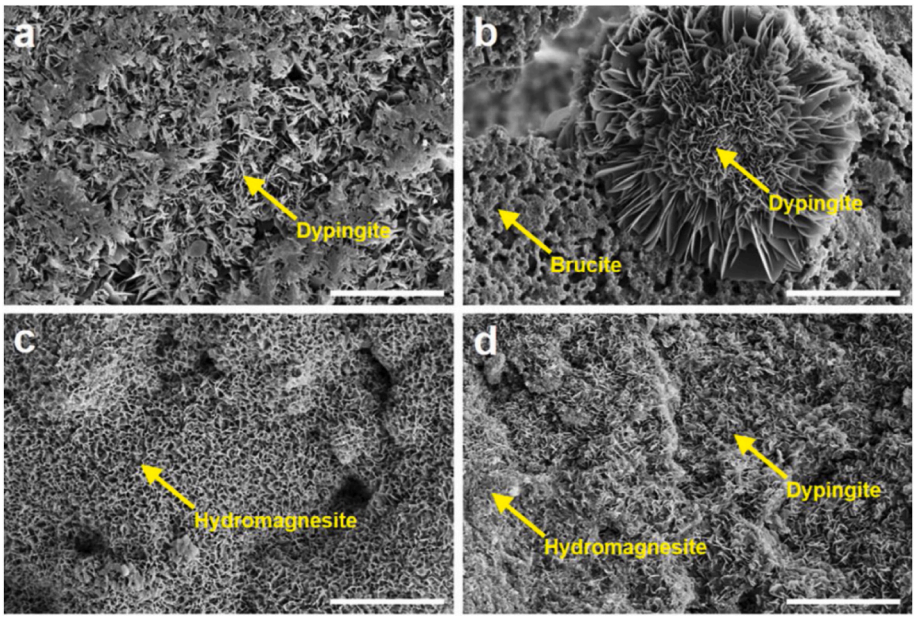


**Fig. 8.** SEM images of (a–b) cast and (c–d) 3D printed RMC samples.
(Images (a) and (c) represent the surface microstructure; (b) and (d) represent the internal microstructure). The scale bar in all images is 10 μm (reproduced from Ref. [25]).

In terms of buildability, the deformation of RMC-$SiO_2$ pastes under the same load was smaller than that of PC pastes at 15 min rest time (Fig. 9), indicating the higher load carrying capacity of the former under the same curing conditions. The improved performance of RMC-$SiO_2$ mixes were associated with the formation of hydrate phases such as *M-S*-H gel, which was investigated via microstructural characterization.

### 3.1.3. *RMC-PC systems*

Another proposed use of RMC is as a partial replacement of PC [63,124,142]. Similar to carbonated RMC systems, the main hydration products of RMC-PC mixes are nesquehonite, brucite, portlandite, magnesite, calcite, calcium silicate and amorphous hydrated Mg-carbonate ($Mg(CO_3)_x(OH)_{2(1-x)}\cdot yH_2O$) [124,142]. An increase in the PC content corresponds to lower brucite and nesquehonite formation, whereas higher RMC contents lead to the domination of the pore structure with brucite, HMCs and other amorphous hydrated Mg-carbonates, which are held responsible for strength development.

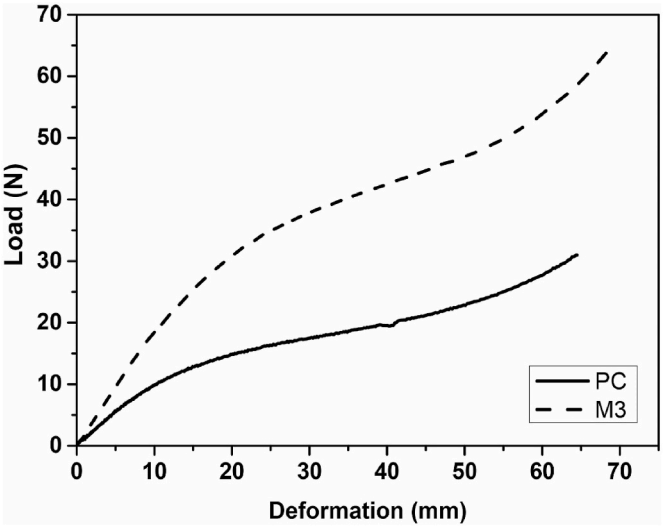


**Fig. 9.** Load-deformation curves of MgO–$SiO_2$ (M3) and PC mixes at 15 min resting time (reproduced from Ref. [141]).

In terms of rheology, owing to its higher specific surface area than PC, the incorporation of RMC increases the water demand and improves the workability of cement-based mixes. RMC-PC mixes containing 30% RMC were reported to have a small dynamic yield stress and plastic viscosity, while their static yield stress was over 4000 Pa [143]. These properties can translate into an efficient extrusion process, after which the printed structure could resist the vertical stress applied by the upper layers.

Although RMC-PC mixes have not been used in 3D printing applications until now, their rheological properties could be assessed via a method proposed by Zhang [143], which is based on the dense accumulation of identical spheres to estimate the water film thickness of the smallest particles in mortar and concrete mixes. The water film thickness calculated by this method could have a good correlation with the rheological parameters of RMC-PC blends. The use of this theoretical method could enable the prediction and modification of the rheological parameters of RMC-PC mixes to meet the fresh properties and performance requirements of 3D printing applications.

## 3.2. *Magnesium phosphate cements*

Magnesium phosphate cement (MPC) is a magnesia-based binder involving the acid-base neutralization reaction between MgO and a phosphate (e.g. ammonium dihydrogen phosphate or potassium dihydrogen phosphate) [144,145]. These binders can set and harden rapidly after contacting with water at room temperature. MPC possesses the advantages of short setting times, high early strengths, good fire and heat resistance, and therefore can be used in the rapid repair of roads and bridges and treatment of radioactive hazardous substances [146–148].

Due to its characteristics such as high setting rates, MPC can meet the basic performance requirements for 3D printing via the modification of its rheological properties by optimizing the mix design or incorporating different admixtures. The increase of MgO to $KH_2PO_4$ (M/P) molar ratio and water glass content can reduce the setting rate of magnesium potassium phosphate cement (MKPC) at high w/b ratios, while the incorporation of FA can increase the setting time and fluidity of fresh MKPC pastes [149,150]. The modification effect of FA on MPC is mainly

associated with its role as a filler and contribution to the chemical reactions. Previous studies [151] reported that the inclusion of 30 wt% FA can improve the fluidity and mechanical properties. An investigation of the influence of different types of phosphates on the rheological properties of MPC concrete revealed that the slump flow of mixes containing $KH_2PO_4$ was lower than those with $NH_4H_2PO_4$, and the decline of the $NH_4H_2PO_4$:MgO ratio further reduced the fluidity of concrete [152]. Amongst the three different admixtures ($Na_2B_4O_7{\cdot}10H_2O$ (NB), $Ca(NO_3)_2{\cdot}4H_2O$ (CN) and $Na_2SO_4{\cdot}10H_2O$ (NS)) used in MKPC pastes, the maximum initial setting time of MKPC mixes was recorded as 37 min when NB, CN and NS were included at a ratio of 1.5%:1.5%:5%, accompanied with a significantly lower hydration exothermic rate [153]. This outcome highlighted a potential way to adjust the rheological properties and extended the open time of MKPC to meet the requirements of 3D printing.

A recent study [154] looked into the use of MKPC pastes in 3D printing. The proposed mixes involved light-burnt MgO and FA as the binder, whose rheological and mechanical properties were adjusted via the addition of SF. Contrary to FA, SF reduced the spread diameter and increased the yield stress and shape compliance of the prepared pastes. MKPC mixes, where MgO was replaced with 60 wt% FA and 10 wt% SF in the presence of borax, revealed enhanced yield stress and prolonged working times, thus enabling their use in 3D printing. Early-age compressive strength test results showed that these samples achieved sufficient strengths (2 MPa at 20 min and 5.36 MPa at 90 min) to prevent deformation due to the upper stacking pressure after extrusion. As can be seen in Fig. 10, the shape of the specimen was highly consistent with the CAD model, resulting in a continuously and uniformly distributed hardened paste. In another study [155], a 3D printing MKPC paste with a M/P mass ratio of 3, incorporating 40 wt% borax and 25 wt% FA show good buildability, with a minimum deformation rate of 0.28% and highest compressive strength of 32.59 MPa. Furthermore, the thixotropy of MKPC was proved to be much higher than that of other cementitious systems, and the incorporation of SF decreased the negative high viscosity of MKPC due to the fast formation of reversible agglomeration [156].

In addition to the mix proportion, the selection of 3D printing craft is also an important factor that affects the performance of printed MKPC components. Fu et al. [157] introduced a process for printing MKPC mixes with a modified binder jetting system. An appropriate nozzle size, mixing and compaction method, as well as framework and retarder requirements were determined as the main printing parameters influencing the final outcome. It was concluded that this binder jetting system had a higher production efficiency and wider applicability when compared with traditional casting.

**Fig. 10.** MKPC sample used for 3D printing (reproduced from Ref. [154]).

### 3.3. Magnesium oxychloride/oxysulfate cements

In order to use magnesia-based cementitious materials effectively, it is necessary to reduce the supersaturation of the suspension system while accelerating the dissolution of MgO in water and improving the solubility of hydration products. Accordingly, using $MgCl_2/MgSO_4$ solution instead of water as the blending agent of MgO, which is similar to the principle of MPC, magnesium oxychloride (MOC)/magnesium oxysulfate (MOS) systems, offers a feasible solution to this issue [158,159]. The application scopes of MOC and MOS include walls, boards, rendering wall insulation panels, and grinding and polishing stones [61]. The main phases present in MOC cements are MgO, $Mg(OH)_2$ and other crystal phases (3 $Mg(OH)_2{\cdot}MgCl_2{\cdot}8H_2O$ (Phase 3) and 5 $Mg(OH)_2{\cdot}MgCl_2{\cdot}8H_2O$ (Phase 5)); while the hydration products of MOS cements are mainly composed of $xMg(OH)_2{\cdot}yMgSO_4{\cdot}zH_2O$ [160–163].

Sinka et al. [164] preliminarily compared some basic properties of four alternative binder systems (MPC, MOC, calcium sulfoaluminate, and gypsum) applied in 3D printing bio-based building materials. Among them, MOC demonstrated the longest initial and final setting times, relatively high compressive strengths and the best compatibility with bio-based fillers. Although the research on the use of MOC/MOS in 3D printing is limited, previous studies have looked into the adjustment of their rheological properties. Additives such as FA can improve the fluidity, decrease the thixotropy (i.e. reduce the volume of flocculation structure), and delay the setting time in fresh MOC pastes through their water absorption effect and morphology [165]. Similar to PC mixes, polycarboxylate superplasticizer (PCE) can significantly improve the rheological properties of MOC pastes due to its adsorption on the surface of cement particles, thus delaying the reaction between MgO particles and water [166]. In MOS systems, the hydrophobic effect of naphthalene superplasticizer (NFS) was shown to work better than PCE, suggesting that NFS is more suitable for MOS mixes [167]. These outcomes can lay the foundation for the adjustment and use of MOC/MOS systems in the field of 3D printing.

## 4. Aluminate cements

### 4.1. Calcium aluminate cements

Calcium aluminum cement (CAC) is an alternative binder with monocalcium aluminate (CA), calcium dialuminate ($CA_2$) and dodecacalcium hepta-aluminate ($C_{12}A_7$) as the main mineral components [76]. When compared with PC, some of the main advantages of CAC include its high abrasion resistance, bacteriological acid corrosion and refractory properties [168–170]. CAC can also be mixed with PC to obtain hardened cement stones with improved durability [171]. Maier et al. [172] studied the 3D powder printing performance of flash-setting CAC. Due to the high chemical activity of $C_3A$ in clinker, it can react with $C_{12}A_7$ rapidly (i.e. flash set), whose reaction lasts only a few seconds. This facilitates rapid setting and strength development of the printed material following nozzle extrusion, guaranteeing that the structure retains high dimensional precision after being stacked on the platform. Once water is injected into the powder bed via the print head, the calcium aluminate phases dissolve in water as $Ca^{2+}$ and $[Al(OH)_4]^-$, raising the pH of the liquid phase. When the water supply during 3D power printing process is sufficient, calcium aluminate hydrate, alumina hydroxide gel ($AH_x$) and crystalline gibbsite ($AH_3$) undergo dissolution, nucleation and precipitation.

Fig. 11 shows the XRD patterns of the printed samples of $C_3A$ and $C_{12}A_7$ with a mass fraction of 1:4, after soaking in water for different durations (0, 24 and 72 h) [172]. The primary hydration products of the non-soaked specimens were reported as $C_3A$ and $C_{12}A_7$, suggesting that the hydration degree of CAC was low at the end of the printing process.

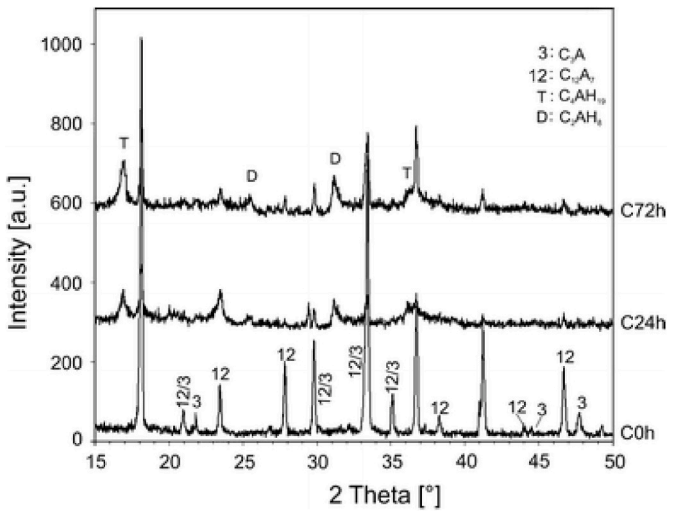


**Fig. 11.** XRD patterns of 3D printed CAC samples under different soaking periods in water (reproduced from Ref. [172]).

As the time immersed in water increased, $C_3A$ and $C_{12}A_7$ gradually began to react and generate $C_2AH_8$ and $C_4AH_{19}$. When combined with FTIR and SEM results, the hydrolysis reaction of 3D printed CAC mixes was found to include the formation of an amorphous hydroxide gel, followed by the crystallization of hydroxide phases. In another study [173], a combination of CAC, PC and lithium carbonate was used as powder material for 3D printing. When the saturation level of shell and core reached 170%, the maximum 28-day compressive strength of the printed cubes was 8.26 MPa. Moreover, porosity and w/b ratio, which are associated with the compressive strength of the prepared mixes, can be adjusted for further strength development. Overall, research has shown that *P*C-CAC mixes can be successfully used in the development of 3D printed structures.

### 4.2. Calcium sulfoaluminate cements

Calcium sulfoaluminate (CSA) cement consists of ye'elimite ($3CaO{\cdot}3Al_2O_3{\cdot}CaSO_4$, abbreviated as $C_4{\cdot}A_3{\cdot}\overline{S}$) and $C_2S$ as the main components [174]. Similar to CAC, CSA cement has minimal $CO_2$ emissions and high resistance to water permeation, carbonation and drying shrinkage, making it a viable candidate for various building applications [175–177].

Chen et al. [178] investigated the early rheological properties of 3D printed CSA cement mixes. The Bingham model and the Herschel-Bulkley (H–B) model were both shown to correctly describe the rheological behavior of CSA mixes. At low shear rates, the static yield stress of CSA cement grew considerably over time. The inclusion of metakaolin can also enhance paste thixotropy and minimize deformation after printing. Ingaglio et al. [179] studied the feasibility of using 3D printing cement and fine aggregates for high resolution binder jet printing. Results showed that the rapid curing ability of CSA improved the accuracy of the 3D printed specimens, while lowering paste segregation. Overall, CSA cement mixes were shown to offer excellent 3D printing characteristics and moderate strengths.

Aside from the mix proportions, the addition of several chemical admixtures can also improve the 3D printing performance of CSA cement mixes. Ding et al. [180] prepared CSA cement mixes for 3D printing by optimizing the hydroxypropyl methylcellulose (HPMC) content, sand content and w/b ratio. The incorporation of HPMC improved not only the shape retention at rest and dynamic rheological behavior of the mixes, but also enhanced the early strength within 2 h [180,181]. By recycling industrial solid wastes (e.g. flue gas desulfurization, carbide slag, aluminum ash, and red mud), Shahzad et al. [182] prepared a sulfoaluminate high-activity material for 3D printing applications. The 3D printing performance of the aforementioned mixes were optimized by adjusting the dosage of boric acid (BA) as a retarder and flowability enhancer, and lithium carbonate as an accelerator. The setting time and fluidity of the optimized mixes were reported as 42 min and 180.7 mm, respectively; whereas the 28-day compressive strength reached 97.5 MPa. However, the addition of excessive BA and sodium gluconate led to structural failure, highlighting the need to control their dosages for successful printing applications [32]. Tartaric acid (TA) was also used to optimize the rheological properties and setting rate of printed CSA mixes [183]. While maintaining the mechanical properties, TA can reduce the deformation rate of printed specimens to less than 10%. Given the characteristics of PC and CSA cement, *P*C-CSA cement mixes with suitable mix proportions could fulfil the extrudability and buildability criteria for the 3D printing process [184].

In addition to their preferrable mechanical properties, the combination of PC and CSA cement can also enhance the interlayer bond strength of the printed samples [185]. Cellulose fiber (CF) was used as an internal curing agent in CSA mixes to retain water for hydration, showing great potential for 3D printing applications [185]. Accordingly, with the inclusion of 1.57 wt% CF at 60 min time intervals, the interlayer tensile and shear strength of CSA samples exceeded 1.91 MPa and 4 MPa, respectively. The microstructural investigation of the hydration products including EDS spectral processing (Fig. 12) revealed the formation of wollastonite, calcium aluminum sulfate hydrate and other hydration products. These phases led to the densification of the microstructure, as well as an increase in the compressive strength of the samples.

## 5. Gypsum-based materials

Gypsum-based materials are particularly appealing in modern structural design due to their benefits such as high fire resistance, lightweight characteristics, and outstanding thermal and acoustic insulation [186]. However, high volume 3D powder printed gypsum still has several issues, mainly associated with its hygroscopicity and agglomeration tendency [187–189]. Therefore, gypsum needs to be stored in a dry environment before printing.

### 5.1. Rheology

Considering the poor fluidity of gypsum-based materials, chemical additives are typically required to enhance their fluidity in order to satisfy the extrusion rate requirements of 3D printing [190]. Amongst the different types of superplasticizers, the adsorption of $\beta$-naphthalene sulfonic acid type (BNS) superplasticizer and PCE on the surface of gypsum particles conforms to Langmuir's adsorption isotherm, exerting steric hindrance effect in gypsum pastes to weaken the degree of particle aggregation and improve fluidity [191]. The distinction is that BNS acts as physical adsorption, whereas PCE is a chemical adsorbent. The adsorption and dispersion of PCE on the surface of gypsum particles can improve the rheological properties [192]. HPMC, however, has a negative effect on the fluidity of gypsum pastes. Given that PCE and HPMC adsorb competitively on the surface of gypsum particles, resulting in an opposing impact on rheological properties, the fluidity of gypsum-based materials can be fully optimized by adjusting the dosages of these additives. On this basis, Liu et al. [186] greatly improved the rheological properties and shape retention ability compared to the original gypsum mix by adjusting the content of PCE, HPMC and starch ether (SE). The dynamic yield stress and final viscosity of the adjusted slurry were reported as 420.73 Pa and 7.29 Pa s, respectively; with a comparable strength to that of the gypsum plaster sample obtained via traditional molding.

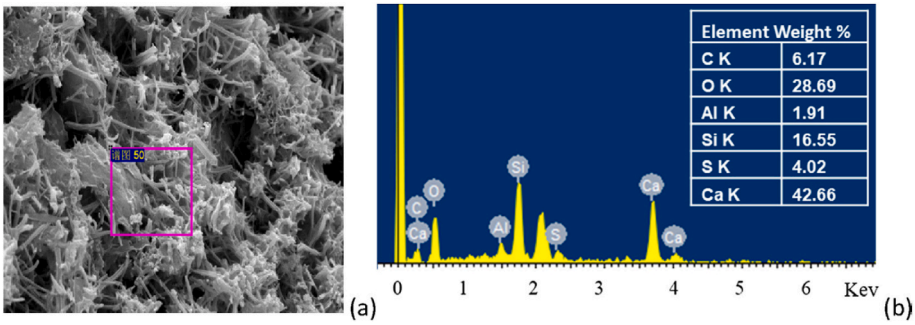


**Fig. 12.** Hydration products of cement mixes containing PC and high belite sulphoaluminate at 28-day, showing: (a) SEM image and (b) EDS results (C═$CaCO_3$; O═$SiO_2$; Al═$Al_2O_3$; Si═$SiO_2$; Ca= Wollastonite) [185].

### 5.2. Application in 3D printing

Unlike other alternative binder systems, gypsum-based materials are usually used to substitute natural rocks, as well as in 3D powder printing applications [193,194]. Kong et al. [194] compared the mechanical properties and microstructure of 3D printed gypsum powder-based rocks and natural rocks. The compressive strength of 60 mm and 120 mm length 3D printed rocks were 7.79 MPa and 3.05 MPa, respectively; which were not as strong as those of many natural rocks (Fig. 13). Printing material and resolution are two important factors controlling the mechanical properties of 3D printed rocks involving gypsum. The proportion of spherical pores in gypsum rocks are larger than that of leaf flakes [195]. From a nano-scale perspective, 3D printed gypsum rocks exhibited typical elastic-plastic behavior in nano-indentation experiments [196], showing similar mechanical properties in different orientations. Hydrophobic silica was reported to improve the fluidity of gypsum powder more effectively when compared with hydrophilic silica [190], which played a key role in 3D printing applications. The gypsum powder layer used in 3D powder printing was smoother and had reduced porosity when 1 wt% hydrophilic nanosilica was added [190]. In addition to being used as building materials, 3D printed gypsum-based materials also find uses as porous cellular sound absorbers [197]. An investigation of the effects of cell structure and porosity on sound absorption coefficient of gypsum-based porous metamaterials revealed a considerable increase in the sound absorption of these materials when compared to non-porous reference specimens.

## 6. Limestone-calcined clay-based cementitious materials

Calcined clay (CC) has a higher pozzolanic activity than FA and GGBS, with limited influence on the early mechanical characteristics of cement-based mixes when used in part to replace PC. Kaolinite-rich clays, which may be found in abundance worldwide, can be quite pozzolanic if calcined between ~700 °C and 850 °C [66,198]. These advantages have increased the interest in CC in recent years [199]. Chen et al. [200] investigated the effects of different grades of CC (i.e. high-grade calcined clay (HGCC) and low-grade calcined clay (LGCC)) on the 3D printing performance, mechanical properties and hydration process of limestone calcined clay cement ($LC^3$) mixes. The total specific surface area of fresh mix particles increased, whereas the average particle distance decreased as the HGCC content increased, leading to increased flow uniformity. At the same time, HGCC improved the buildability of the mixture, which could be due to the enhancement of particle flocculation and increased water adsorption. As shown in Fig. 14, the highest number of layers that HCC mixes consisting of 40 wt % PC, 20 wt% LGCC, 20 wt% HGCC and 20 wt% limestone powder (LP) could be stacked without any obvious structural deformation was 21, indicating that the buildability of this mix fulfilled the criteria for 3D printing. The corresponding number for mixes with LGCC as the alternative binder (LCC) was reported as only 9 layers. The actual printing heights of the mixtures investigated in this study were all much lower than the theoretical height under the effects of cumulative deformation and elastic buckling of the layer-by-layer printed structure. Increased metakaolin concentration in calcined clay can also cause large increases in extrusion pressure, which may be related to the acceleration of the hydration rate of the system [201].

Similar to aluminate cements and gypsum-based materials, PCE and HPMC can also significantly affect the 3D printing performance of *PC–CC–LP* mixes [202,203]. When 0.24% HPMC-based viscosity-modifying admixture (VMA) was incorporated, the modified mixture had better shape retention, buildability and 7-day compressive strength than other groups. Within this system, the use of higher amounts of VMA

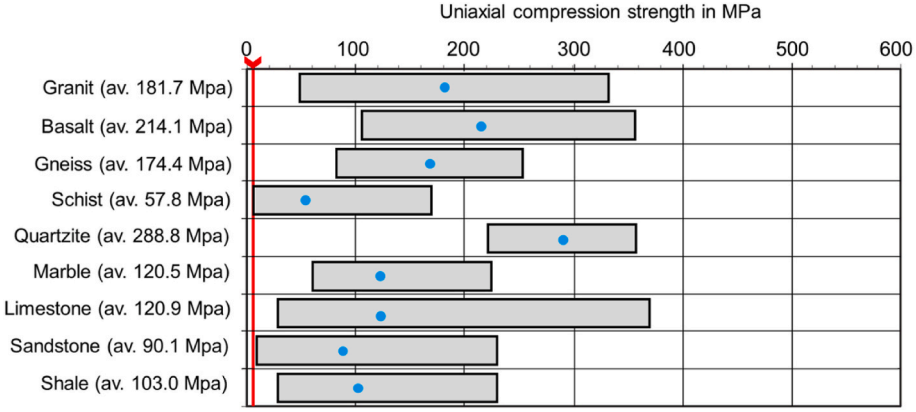


**Fig. 13.** Compressive strength of different types of rocks and 3D printed gypsum rock. (The grey box indicates the range of compressive strength for various rocks; the blue dots represent their average value; the red line is the compressive strength of printed gypsum rock with a length of 60 mm) (reproduced from Ref. [194]). (For interpretation of the references to colour in this figure legend, the reader is referred to the Web version of this article.)

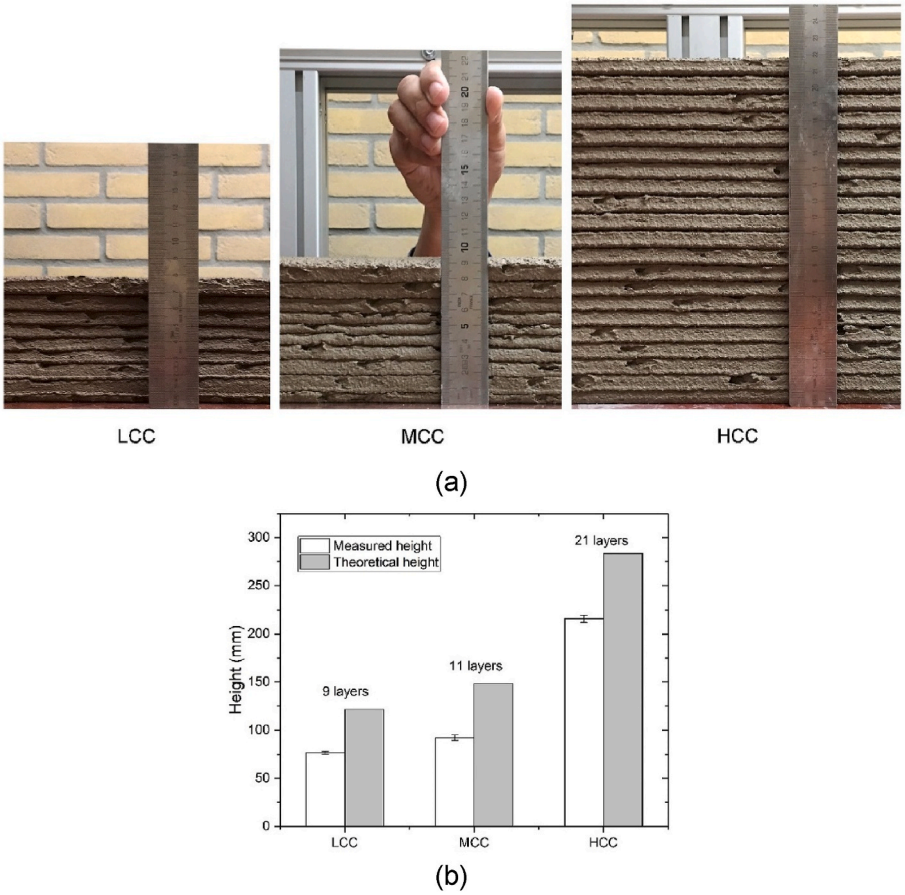


**Fig. 14.** Buildability tests of *PC*–CC–LP ternary mixes (LCC: 40 wt% PC + 40 wt% LGCC + 20 wt% LP; MCC: 40 wt% PC + 30 wt% LGCC + 10 wt% HGCC + 20 wt% LP; HCC: 40 wt% PC + 20 wt% LGCC + 20 wt% HGCC + 20 wt% LP), showing: (a) buildability performance and (b) height and layer number (reproduced from Ref. [200]).

increased the extrusion pressure [204] and delayed the hydration rate of composite pastes by affecting portlandite precipitation and *C*–S–H adsorption [202].

Among all the printing parameters, the nozzle standoff distance and time interval were reported as some of the most critical parameters that affect the mechanical properties of 3D printed $LC^3$ samples [205]. When the time interval increased from 1 min to 10 min, the interlaminar bond strength of the printed specimen decreased by 13% when compared with cast samples, owing to an increase in local porosity. Changing the standoff distance only had a very limited influence on the bond strength, but raised the risk of inaccurate layer deposition [205].

## 7. Other binders

In addition to the aforementioned binder systems, there are other cementitious materials used as binders instead of PC in 3D printing. One of these is raw earth that has been used as a building material since the Middle Bronze Age (XIV Century B.C.) [206]. In spite of its long history, only a few studies have been conducted on the 3D printing of earth-based materials. Perrot et al. [207] reported a preliminary assessment of employing earth-based materials in 3D printing process. Adding alginate to the soil could improve the green strength of these mixes. The compressive strength of printed samples was very close to that of the traditional earth-based materials, indicating that the printing technique did not dramatically decrease their mechanical performance. In order to achieve high insulating capabilities, Dubois et al. [208] incorporated quarry fines as earth-based components into 3D printed lightweight composites with gypsum and natural prompt cement as the major binder. The developed mixes were well suited for 3D printing due to their sufficient workability and quick hardening, enabling them to withstand their own weight.

Copper and iron tailings are two industrial wastes produced after crushing and beneficiation of copper and iron ores, respectively [209, 210]. Reasonable recycling of these two materials in a responsible manner can assist to safeguard the environment and save land resources. By adjusting the amount of iron tailings, copper tailings, FA and belite cement, the fluidity of the prepared mortars can meet the requirements of 3D printing [211]. The ideal mass ratio of copper tailings to iron tailings was reported as 1:4, at which the mixture achieved maximum compressive strength (45.2 MPa at 28 days), associated with the formation of *C*–S–H gel and ettringite (AFt) as the primary hydration products [211].

High-volume FA mixes, where the FA content exceeds PC, resulting in a reaction between $SiO_2$, $Ca(OH)_2$ and high alkaline hydrated calcium silicate, are also considered as an alternative binder system. The thixotropy of high-volume FA mixes could be enhanced via the addition of nano-attapulgite clay, owing to an increase in flocculation strength under the action of nano-attapulgite clay, thus making them more suitable for concrete printing applications [212]. Similar to nano-attapulgite clay, micro-silica can also improve the buildability and strength development rate of FA mixes [213]. While these materials may contribute to the printing quality of high-volume FA mixes, their composition and mix design can be further tuned, based on specific geometrical and mechanical criteria.

The environmental impact of construction and demolition waste has become a major concern in the construction industry. To address this issue, some of the construction waste is reused as recycled aggregates or powders in new structures. The development of alternative binders from

recycled powders can reduce the use of PC. Duan et al. [214] and Hou et al. [215] examined the rheological properties and 3D printing features of mortars incorporating recycled powders derived from demolition wastes of brick-concrete buildings, respectively. The inclusion of recycled powders was reported to increase the yield stress, plastic viscosity, and thixotropy; and improve the hydration exothermic rate of the original PC pastes within 30 min. Simultaneously, recycled powders could enhance the extrudability and buildability of 3D-printed mortars, as well as boost their strength and Young's modulus at early stages. These findings demonstrate that the recycling and reuse of recycled powders may not only contribute to the sustainability of construction materials, but also enhance the performance of 3D printing processes.

## 8. Comparison of alternative binders to PC for 3D printing applications

Various mix proportions of geopolymers/alkali-activated systems, MgO-based cements, CAC/CSA cements, gypsum-based materials, and $LC^3$ have been reported in the context of 3D printing. The mechanical properties of these mixes with different raw materials, printing systems and curing conditions are detailed in Table 1. Given the variety of rheological parameters and hydration degree calculation methods, it is challenging to quantitatively describe the rheological [216–219] and hydration [220–223] processes of these various binders using a single set of characteristic parameters. Therefore, the rheological and hydration properties are not provided in Table 1. Fig. 15 presents images of the typical printed samples of alternative binders addressed in this paper to highlight their characteristics. Meanwhile, the in-depth review performed in this paper led to the preparation of a comprehensive framework highlighting the advantages, disadvantages and near-future directions of the use of various alternative binders in 3D printing applications, as shown in Fig. 16.

As an emerging and promising building material, geopolymers are currently being optimized for their mechanical properties and durability. Whether cast or 3D printed, geopolymers can achieve compressive strengths comparable to PC samples by adjusting the type and concentration of the alkaline activator, Si/Al ratio, Na(K)/Al ratio and water consumption; presenting a potentially higher rate of strength development at early ages. In terms of durability, geopolymers present a high thermal stability due to their special silicon oxygen tetrahedron structure [224] and are more durable than *P*C-based mixes in both acidic and alkaline media (i.e. particularly in terms of their sulfate resistance) [225]. These advantages play a key role in the development of geopolymer-based prefabricated components via 3D printing, which can be manufactured indoors and then utilized in environments with high durability requirements.

Despite possessing reasonable compressive strengths, the tensile strength and fracture toughness of geopolymers are inadequate, which can be improved via the addition of fibers [226]. AAS mixes also demonstrate high volume shrinkage throughout the setting and hardening processes, which can result in the ingress of corrosive ions into the samples along the shrinkage cracks, thereby compromising their impermeability [227]. In terms of their suitability for the 3D printing process, the rheological properties of geopolymers can be adjusted via the addition of CMS to enable their smooth and uniform extrusion from the nozzle, followed by the ability to withstand stress from the upper layers without deformation, as discussed in Section 2.1.

The most remarkable advantages of RMC-based binders over PC are the lower calcination temperatures needed for their production, ability to be recycled and reused at the end of their lifetime and alternative production routes. MgO, the main component of RMC, can come from magnesite (dry-route) or reject brine or seawater (wet-route), with abundant reserves on a global scale [61]. In carbonated RMC systems, the carbonation process of brucite ($Mg(OH)_2$) to generate HMCs enables the storage of $CO_2$ produced during the production process ($MgCO_3 \rightarrow MgO + CO_2$), resulting in a low $CO_2$ binder, depending on the degree of carbonation and source of $CO_2$. As RMC mixes mainly rely on accelerated carbonation for strength gain, in order to use RMC in 3D printing, the printed samples need to be subjected to carbonation conditions for subsequent curing. For *M-S*-H based mixes, their lower internal pH in comparison with the PC system (10.5 vs. 12.5) presents a suitable environment for natural fiber reinforcement [141]. From the perspective of rheological properties and reactivity of the fresh paste, RMC has a faster early hydration rate than PC clinker ($C_3S$ and $C_2S$), which corresponds to a more effective structural build-up. This property can lead to the production of printed samples, whose dimensions are highly compatible with the CAD model.

CAC combines the advantages of geopolymers and RMC-based cements. CAC mixes possess higher early strengths and improved durability aspects such as enhanced resistance to sulfate attack and abrasion [76]. Similar to RMC, the production of CAC can emit less $CO_2$ than PC, contributing to the production of sustainable 3D printed components. Due to the flash setting characteristics of CAC, its use in 3D printing can realize rapid solidification and development of initial strength. On the other hand, CSA cements can either be used alone as a clinker or in combination with PC to form a hybrid binder system. Although CSA demonstrates rapid strength gain at early ages, it may expand with the extension of curing time, presenting concerns over volume stability. However, when compared to CAC and PC, CSA mixes can present advantages in terms of the extrudability and buildability aspects of 3D printing by enabling an increased yield stress of the printed layers [178, 228].

Gypsum-based materials are lightweight, high-strength, fireproof and physically stable, making them suitable for a variety of scenarios. However, in high humidity environments, agglomeration of gypsum can reduce the overall strength, leading to poor water resistance. This aspect also presents a challenge when gypsum is used in 3D printing, making it a viable option for indoor applications such as internal partition walls, wall claddings, ceilings and sound-absorbing boards [197]. Current studies focusing on the extrudability and buildability of gypsum-based mixes for 3D printing purposes should work towards optimizing their rheological properties to broaden the application scope of gypsum in the realm of 3D printing.

$LC^3$ is a relatively newly developed and popular cementitious material, which benefits from the higher pozzolanic activity presented by CC in comparison to FA and GGBS [66]. The replacement of PC with CC and LP does not affect the mechanical performance and can lead to improved durability. However, with the increase of CC and LP content, the fluidity of $LC^3$ decreases, which is the main issue impeding its widespread use in 3D printing [229]. While the increase of HGCC content can improve the buildability of $LC^3$, in the process of improving buildability, attention must also be paid to controlling the extrusion pressure of the material. Large extrusion pressures may reduce the printing speed and even cause nozzle blockage, which will affect the uniformity of the printed sample.

One of the main reasons for the development of alternative binders is their potential to offer lower carbon footprints than PC mixes. For instance, alkali-activated materials and RMC-based mixes can reduce $CO_2$ emissions associated with the calcination of PC clinker due to the use of SCMs and their carbon sequestration potential during their curing process, respectively. However, research has also shown that alkaline activators such as sodium silicate and sodium hydroxide are the primary contributors to carbon emissions for alkali-activated materials. Alternatively, the primary drawbacks of RMC-based mixes involve the lack of understanding of their reaction mechanisms and the limited carbonation they offer under ambient conditions. Furthermore, the use of coal in the calcination of magnesite for RMC production has adverse effects on human health. These issues highlight the need for a detailed evaluation of the environmental impacts of these binders through their life cycles to reveal the most suitable applications for each formulation.

**Table 1**
Properties of alternative binder mixes developed for 3D printing applications.

| Binder name | Raw materials | | | Printing system | Curing conditions (temperature and relative humidity) | Compressive strength (MPa) | | | Flexural strength (MPa) | | | Ref. |
|---|---|---|---|---|---|---|---|---|---|---|---|---|
| | Main component | Admixtures and fibers | Aggregates | | | 3-day | 7-day | 28-day | 3-day | 7-day | 28-day | |
| Geopolymers/ alkali-activated systems | GGBS, calcium carbonate, CMS | $Na_2O$ and $SiO_2$ | – | Gantry | 23 °C; 90% | 15–18$^{P}$ | 16–25$^{P}$ | 35–63$^{P}$ | 3.6–4.0$^{P}$ | 5.3–5.4$^{P}$ | 5.5$^{P}$ | [93] |
| | Graphene oxide, metakaolin | Sodium silicate, sodium hydroxide, | – | Gantry | 25 °C + 45% | – | – | 173–202$^{P}$ | – | – | – | [238] |
| | FA | 10 M sodium hydroxide solution, sodium silicate solution, green tow flax fibers | Sand | Injected process | 75 °C for 24 h, unmolded for 7 days | – | 39.6–47.1$^{P}$ | – | – | 7.1–7.4$^{P}$ | – | [239] |
| | FA, GGBS, SF | Potassium hydroxide, potassium silicate solutions | Fine river sand | Gantry | Ambient curing | – | 19.6–22.1$^{P}$ | 33.2–36.3$^{P}$ | – | – | 4.7–9.6$^{P}$ | [240] |
| | FA, GGBS, nanoclay | Hydroxide and silicate solutions of potassium | River sand | Gantry | 23 ± 2 °C | – | – | 22.7–32$^{C}$ | – | – | – | [87] |
| | FA, GGBS, SF | sodium silicate solution, 45 wt% NaOH solution | River sand | Gantry | 25 ± 2 °C | – | 18.4$^{P}$ 16.2$^{C}$ | – | – | – | – | [91] |
| | FA, GGBS | Liquid potassium silicate | Fine river sands | Gantry | 25 ± 3 °C | – | – | 36$^{P}$ | – | – | 5.05$^{P}$ | [108] |
| | FA, GGBS, SF | Penta sodium metasilicate (PSM) powder, microcable | Sand | Robot | Room temperature | – | – | 23.2–41.5$^{P}$ | – | – | – | [105] |
| | FA | NaOH solution, sodium silicate | Sand | Injected process | 75 °C for 24 h, standard curing | – | 39.5–47$^{P}$ | 38.5–48$^{P}$ | | 7.1–7.7$^{P}$ | 6.9–9.3$^{P}$ | [107] |
| | GGBS, plaster | Silicate-based activator | Fine sand | Powder printing | – | – | 15.7–16.5$^{P}$ | – | – | – | – | [241] |
| | FA, GGBS | Sodium silicate, potassium silicate solutions | Silica sands | Gantry | 23 ± 3 °C | 8.5–16.6$^{P}$ | 13.1–21.1$^{P}$ | 19.8–34$^{P}$ | – | 4.4–5.8$^{P}$ | 6.3–7.1$^{P}$ | [97] |
| | FA | Saturated anhydrous sodium metasilicate solution, NaOH solution, sodium silicate solution | – | Powder printing | 25 °C, 40 °C, 60 °C, 80 °C | 2.3–26.4$^{P}$ | 2.2–29.6$^{P}$ | – | – | – | – | [242] |
| | GGBS | Ground anhydrous sodium metasilicate powder | Fine silica sand | Powder printing | 60 °C for 7 d, 23 °C + 65% Immersed in Na-based solutions and K-based solution | – | 7.6–29.6$^{P}$ | 9.8–27$^{P}$ | – | – | – | [243] |
| | FA, GGBS | Anhydrous sodium metasilicate powder | Silica sand | Powder printing | 60 ± 3 °C for 7 d, Immersed in Na-based alkaline solution | – | 6.1–29.6$^{P}$ | – | – | – | – | [102] |
| | FA, GGBS | Potassium silicate powder, potassium hydroxide (KOH) powder | Fine river sand | Gantry | Ambient curing | – | – | 24.5–28$^{P}$ | – | – | – | [96] |
| | FA, GGBS, SF | 98% pure NaOH, sodium silicate, Nano-graphite platelets | River sand | Gantry | 60 °C for 24 h, 20 °C | – | 40–48$^{P}$ 44–67$^{C}$ | – | – | 8–11.8$^{P}$ 9–11.2$^{C}$ | – | [99] |
| | FA, GGBS, PC, LP, Alumina powder | NaOH, sodium silicate solution, $Na_2SO_4$ | – | Desktop printer based on Cartesian configuration | 23 ± 1 °C, >98% | – | – | 4–31$^{P}$ | – | – | 1.1–4.3$^{P}$ | [88] |
| MgO-based cements | RMC, caustic MgO | 0.1 M magnesium acetate aqueous solution, polycarboxylate ether, defoamer, suspension aid additive | Standard sand | Gantry | 22–23 °C; 56–59% for 3 d carbonated for 7 d | – | 31$^{P}$ 16$^{C}$ | – | – | – | – | [25] |

(*continued on next page*)

**Table 1** (*continued*)

| Binder name | Raw materials | | | Printing system | Curing conditions (temperature and relative humidity) | Compressive strength (MPa) | | | Flexural strength (MPa) | | | Ref. |
|---|---|---|---|---|---|---|---|---|---|---|---|---|
| | Main component | Admixtures and fibers | Aggregates | | | 3-day | 7-day | 28-day | 3-day | 7-day | 28-day | |
| | RMC, microsilica | Sodium hexametaphosphate (SHMP) | – | Gantry | 30 ± 2 °C; 60 ± 5% | – | – | 36.2–44.3$^{C}$ | – | – | – | [141] |
| | caustic MgO | Magnesium chloride salt solution | – | Gantry | 20 ± 2 °C; 50 ± 10% | – | 57.1$^{C}$ | 75.2$^{C}$ | – | – | – | [164] |
| Aluminate cements | PC, CAC | Lithium carbonate | – | Powder printing | Room temperature; Saturated in water/$Ca(OH)_2$ solution | – | 0.7–3.6$^{P}$<br>2.8–14.6$^{C}$ | 1.02–8.26$^{P}$<br>5–19$^{C}$ | – | – | – | [173] |
| | Flue-gas desulfurization gypsum, carbide slag, aluminum ash, and red mud | Boric Acid, Lithium Carbonate | – | Extrusion system | 20 °C; 95% | 41.4–77.4$^{C}$ | 55.6–95.7$^{C}$ | 73.5–125.9$^{C}$ | – | – | – | [182] |
| | CSA | Water-soluble Polymer, surfactant | Silica sand | Binder jet | Air curing for 24 h; water curing | – | 4.9–5.1$^{P}$<br>10.2–12.6$^{C}$ | 5.9–6.7$^{P}$<br>11.9–15.7$^{C}$ | – | – | 1.8–2.4$^{P}$<br>3.1–3.9$^{C}$ | [179] |
| | PC, CSA | Polyvalent non chlorate acrylic copolymer superplasticizer | Calcareous 0/2 mm crushed sand | Simulated by manual process | 20 °C; 100% | – | 64–70$^{P}$<br>77–78$^{C}$ | 78–82$^{P}$<br>87–89$^{C}$ | – | – | – | [184] |
| Gypsum-based materials | α-hemihydrate gypsum | PCE, HPMC, SE | – | Robot | 25 °C | – | – | 65$^{P}$<br>59.6–63.8$^{C}$ | – | – | 15.2$^{P}$<br>14.6–15.8$^{C}$ | [186] |
| LC$^{3}$ | PC, LP, CC | Superplasticizer, viscosity modifying admixture | Sand | Concrete printing | 20 ± 2 °C, 99% | – | 33–49.5$^{P}$<br>27–37.2$^{C}$ | – | – | – | – | [200] |
| | PC, LP, CC | PCE, HPMC | Sand | Concrete printing | 20 ± 2 °C, 99% | – | 18.8–49.5$^{P}$<br>56$^{C}$ | – | – | – | – | [202] |
| | PC, LP, CC | PCE, HPMC | Sand | Concrete printing | 20 ± 2 °C, 99% | – | 11–36.5$^{C}$ | 13–47.5$^{C}$ | – | – | – | [201] |

$^{P}$ Printed samples; $^{C}$ Cast samples.

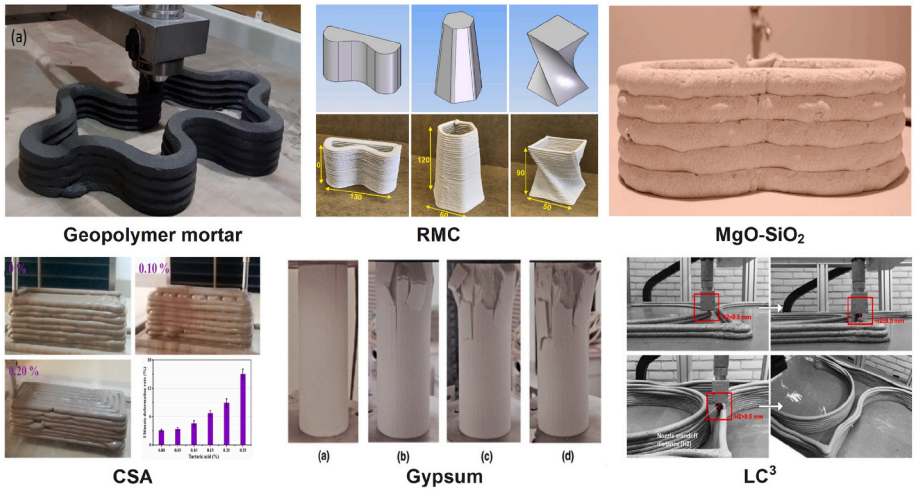


**Fig. 15.** 3D printed samples containing typical alternative binder mixes [25,141,183,194,200,244].

| Binder systems | Advantages | Disadvantages | Future actions |
|---|---|---|---|
| Geopolymers/ alkali-activated systems | Low hydration heat; good heat, sulfate and acid resistance; use of industrial wastes | Use of caustic activating solution; challenging rheology; volume shrinkage; | Enabling the use of industrial wastes in a wide spectrum of applications to replace PC; improvement of rheological properties to meet the requirements of 3D printing |
| MgO-based cements | Production from alternative routes involving waste materials/by-products; capability for strength gain via $CO_2$ sequestration (RMC); good thermal insulation and fire resistance (MOC/MOS) | Poor water resistance (MOC/MOS); fast setting rate causing nozzle clogging (MPC); need for accelerated carbonation curing to gain strength (RMC); poor volume stability (M-S-H) | Improvement of the manufacturing process of MgO clinker; determination of the mechanisms of performance enhancement; development of respective application areas for specific uses |
| Aluminate cements | Low $CO_2$ emissions during production; rapid strength gain; sulfate resistant (CAC); no alkali–silica reaction (CAC); shrinkage compensating (CSA) | Strength loss on conversion of hydrates (CAC); potentially expansive nature (CSA) | Reduction of the cost of clinker manufacturing; production of the raw materials by using wastes; improvement of the stability of hydration products; controling the volume stability of the hardened paste |
| Gypsum-based materials | Lightweight; high strength; fireproof; volume stability | Poor water resistance | Improvement of water stability; development of specific application fields |
| $LC^3$ | Widely available raw materials; low $CO_2$ emissions during production; low cost; good resistance to chloride penetration | Challenging rheology; unproven durability | Further understanding of reaction mechanisms and performance development; improvement of rheological properties to meet the requirements of 3D printing |

**Fig. 16.** Framework indicating the main characteristics and future direction of 3D printed alternative binder systems in construction.

## 9. From lab-scale to large-scale 3D printing construction applications using alternative binder systems

In addition to the potential environmental benefits of alternative binders, 3D printing concrete technology itself has the capability to improve productivity and reduce the environmental impact of traditional construction practices. Previous studies that performed a life cycle assessment analysis on four typical case scenarios (i.e. a traditional cast concrete structure, 3D-printed concrete with reinforcement, 3D-printed concrete without reinforcement and 3D-printed concrete without reinforcement using lightweight materials) demonstrated that 3D concrete printing could significantly reduce the environmental impact of traditional construction methods on GWP, acidification potential (AP), eutrophication potential (EP), smog formation potential (SFP), and fossil fuel depletion (FFD) [230]. Another study also showed that 3D printing houses could be an economically viable option when compared to their conventional counterparts, through the analysis of a single-story 3D printing house [231].

Although numerous laboratory-based studies on several aspects such as mix proportions and mechanical characteristics of formulations involving alterative binders have been performed, several challenges must be resolved before they can be used in 3D printing applications on a large scale [232,233]. Unlike research organizations, which mostly conduct experiments on a laboratory scale, construction companies are generally involved with structures considerably larger than laboratory models. Therefore, in addition to controlling key factors such as mix design and curing conditions, the applied construction technology and process parameters of large printing equipment need to be considered to enhance the dimensional accuracy of structures on a large scale [234].

Traditional systems involving PC are still frequently used in scaled up 3D printing applications. Amongst the various companies working on producing large-scale structures via 3D printing, Total Kustom has

adopted a contour printing technology to print the walls and columns of structures on construction sites (Fig. 17(a)) [235]. After the printed structure is hardened and the dimensional accuracy meets the requirements, concrete is poured into the surrounding area. Similarly, Hebei University of Technology has printed a 5 cm thick formwork, in the middle of which reinforcement was added, followed by the pouring of concrete to form an integrated structure (Fig. 17(b)) [236].

Southeast University and Nanjing Institute for Intelligent Additive Manufacturing jointly developed a method based on a 3D printing elements technology to manufacture a 5.15 m high building with a mix that contained polypropylene fibers (Fig. 18(a)) [235]. The fluidity and slump of these mixes were reported as 230 mm and 55 mm, respectively. These results provided a basis for determining a reasonable workability range for cement mixes to be used in future 3D printing projects. Furthermore, on the Beichen Campus of Hebei University of technology, a 3D-printed concrete arch bridge with a single span of ~18 m has been constructed using various technical innovations. As shown in Fig. 18(b), the aesthetics and structural precision of the printed bridge fulfill stringent criteria.

Despite the fact that only a few alternative binders have been used in large-scale 3D printing applications, some studies have demonstrated relatively large-volume printing attempts in laboratory settings, laying a crucial basis for further industrial developments. Geopolymer systems involving FA and GGBS as the main precursor have demonstrated good extrudability and buildability via the adjustment of their mix proportions [237]. An example to this is a 3D-printed column with 94 layers and a total height of 940 mm, shown in Fig. 19, that was printed after the mix proportion parameters (i.e. w/b ratio, activators and retarder content) were optimized. It can be seen from Fig. 19 that the printed layers did not demonstrate any deformation when subjected to the stress of upper layers. A small difference between the actual structure size and the target size was achieved, validating the buildability of geopolymer-based mixes. The progress made in this area so far has highlighted that establishing a link between lab-scale research and large-scale initiatives can pave the way for the use of alternative binders in the development of 3D printed structures. However, further technical challenges such as the short printable time window of geopolymers, which limits their application in large-scale printing projects, still remail to be resolved.

## 10. Conclusions and recommendations

When compared to traditional curing methods, 3D printing presents a smart, sustainable and customizable building technology involving a range of cementitious materials. The development of customizable alternative binders for 3D printing applications will fuel the rapid expansion of the manufacturing and construction industries on a global scale. Presenting a detailed review of the recent advances in this field, this paper highlights the research progress in alternative binder systems including geopolymers/alkali-activated systems, MgO-based cements, aluminate cements, gypsum-based materials, and $LC^3$ in the context of 3D printing. As a part of this review, the rheological properties, hydration characteristics, reaction products and mechanical properties of each binder type from the perspective of 3D printing were systematically analyzed. This was followed by a discussion on their advantages and disadvantages in comparison with the use of traditional *P*C-based mixes in 3D printing. The information and recommendations presented in this paper aim to guide and benefit different users ranging from academics to construction industry practitioners and policy makers interested in enhancing the sustainability of the built environment and the productivity of the construction industry.

After evolving for hundreds of years, PC still occupies the most important position among cementitious materials due to its established manufacturing process and stable performance. But overall, the most remarkable advantage of alternative binders over PC is their potentially more sustainable production routes, translating into the preservation of natural resources and reduced carbon emissions in the construction industry. The review has led to the identification of possible future development trends involving these binder systems. Specific conclusions can be drawn as follows.

1. Geopolymers/alkali-activated systems have been investigated further than most other alternative binder systems, revealing detailed information on their reaction and strength gain mechanisms. The extent of this information has provided a strong theoretical basis for the promotion of 3D printing applications involving these binders. Geopolymers can offer more heat and sulfate resistance than PC, which can further contribute to their increased use. However, the rheological properties (i.e. shape retention ability) of these mixes still need to be improved. Current research shows that 3D printed geopolymers with FA and GGBS as their main binder can meet the pumping and extrusion requirements, but their buildability is generally lower than corresponding *P*C-based mixes. In this case, it is necessary to add an appropriate amount of SF or adjust the properties (e.g. type, concentration, Si/Al and Si/Na ratio) of the alkaline activator. For AAS, the effect of drying shrinkage on the stability of the printed components should be considered as well. Furthermore, alkaline activators such as NaOH and $Na_2SiO_3$ are expensive and have environmental and health side effects, necessitating special care in their use.
2. The development and application of MgO-based binders are mainly from an environmental perspective, which is also in line with the characteristics of 3D printing technology itself (i.e. saving energy and reducing labor consumption). 3D printed RMC mixes have been shown to achieve nearly twice as high strengths as that of cast samples under the same mix proportion, as well as *P*C-based mixes. Adding an appropriate amount of caustic MgO into carbonated RMC mixes can improve the shape retention ability and the overall integrity during layer-by-layer stacking. In contrast, the greatest advantage of *M-S*-H and MKPC systems is their comparable mechanical properties to RMC without relying on carbonation curing. To improve researchers' and practitioners' confidence towards MgO-based formulations, it is necessary to optimize the present MgO production process, clarify its performance under different conditions, identify suitable reinforcement options for structural applications and verify environmental advantages via a detailed life cycle assessment.
3. Owing to the rapid reaction rate of $C_3A$ and $C_{12}A_7$ in CAC, extrusion-based 3D printing may result in fresh CAC setting before it is extruded from the nozzle, thus affecting its extrudability. As a result, CAC is frequently employed in the field of powder printing. Furthermore, the compressive strengths of printed CAC samples are relatively low, limiting their application. Alternatively, a higher number of studies and practical examples have been reported on 3D printed CSA cement. In general, CSA mixes can possess ideal printability and reasonable mechanical properties via the optimization of

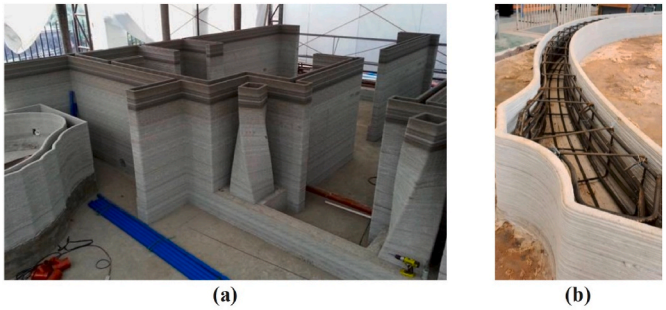


**Fig. 17.** Structures built by 3D formwork printing (i.e. contour crafting), showing: (a) Formwork obtained by TotalKustom and (b) bridge elements manufactured by Hebei University of Technology (reproduced from Ref. [235]).


**Fig. 18.** Large-scale 3D printed structures, showing: (a) 3D-printed fabricated building in Nanjing and (b) 3D-printed concrete bridge in Hebei, China (reproduced from Refs. [235,245]).

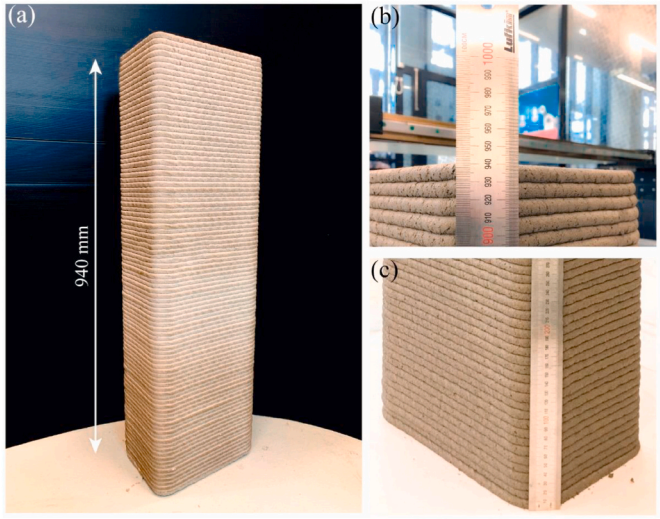


**Fig. 19.** A large volume 3D-printed geopolymer column structure, showing: (a) structural schematic diagram of 940 mm high 94 layers, (b) enlarged view of the top layer and (c) enlarged view of the bottom layer (reproduced from Ref. [237]).

their mix proportions and incorporation of chemical additives such as HPMC, BA and TA. *P*C-CSA mixes can also be used as a binder and form wollastonite, calcium aluminum sulfate hydrate and other hydration products that can significantly improve their interlayer bond strength.

4. Despite having a long development history, the main reason why gypsum-based materials are not widely used in the field of 3D printing is associated with gypsum's tendency to agglomerate after getting damp and its poor fluidity. However, the rheological properties and shape retention ability of gypsum-based materials have been greatly improved by adding additives such as polycarboxylate superplasticizer, HPMC and SE. Similar to CAC, gypsum-based mixes also use powder printing technology for the production of 3D printed components. At present, its main applications involve the replication of natural rocks and as a porous cellular sound absorber.
5. $LC^3$ is a recently emerging alternative binder, which is claimed to not only reduce the carbon emissions caused by clinker production, but also involve the use of clay, which is commonly found in different parts of the world and can be calcined in an affordable manner. The buildability of $LC^3$ mixtures is significantly enhanced as the HGCC content increases, allowing the stacking of 21 layers vertically without collapsing. The nozzle standoff distance and time intervals are the two most influential printing parameters in the production of 3D printed components with $LC^3$.
6. Recent research has revealed that earth-based materials, copper tailings, iron tailings, high-volume FA mixes, and recycled powders can also be used as alternative binders in 3D printing. Although only a limited amount of research has been performed in this area so far, the use of these materials as cementitious materials enables waste utilization. High-volume FA mixes present a potentially viable alternative binder option when the source of raw materials and the strength of hardened pastes are taken into account. The thixotropy, buildability and strength development rate of high-volume FA mixes can be significantly improved via the addition of nano-attapulgite clay and micro-silica.

In large-scale 3D printed concrete applications, cementitious binders should be optimized for more cost-effective and environmentally-friendly construction projects. At present, in addition to PC, geopolymers/alkali-activated materials are the main binders closest to large-scale 3D printing applications. Results obtained so far have shown that the buildability of concrete mixes can be remarkably enhanced by reasonably optimizing the mix proportions and adjusting the workability parameters, resulting in a considerable improvement in the dimensional accuracy of the printed structure. Since there are different technical routes and equipment requirements for large-scale 3D printing, the workability requirements for lab-scale 3D printing cannot be entirely applied to large-scale applications and need to be adjusted in line with the approach adopted. To optimize the mix proportions of alternative binders, it is also necessary to consider the selection of technical route, the specific features of the printing equipment and control systems, and the modification of printing parameters.

In order for these alternative cementitious materials to extensively substitute *P*C-based systems and enable their application in projects with different performance requirements, there are several challenges that need to be overcome. Initially, the lack of sufficient documentation and limited familiarity of the industry with these systems present a barrier. Furthermore, the lack of widespread expertise required for optimizing key factors such as the mix proportion and performance of alternative binder systems for different environments results in a low market confidence in these emerging materials.

Geopolymers/alkali-activated materials are some of the most well-know and researched alternative binder systems. However, the composition, particle morphology, particle size distribution and chemical activity of the main components (e.g. FA and GGBS) show variations in different locations and even batches from the same facility. These variations are due to the waste natures of these materials, along with the numerous unknown elements in their production process and source of raw materials. Further detailed investigations form a critical step toward achieving standardization in the context of 3D printing.

Similarly, although certain MgO-based systems have been reported to possess comparable mechanical properties to PC and high durability, the variation amongst MgO sources (i.e. dry-route involving the

calcination of magnesia-based minerals or wet-route involving extraction from brine or seawater) causes differences in the physicochemical properties of MgO. Alternatively, the low strength gain of CAC/CSA cement and poor water resistance of gypsum restrict their widespread use in 3D printing. Differing from these systems, the cost of raw materials and production of $LC^3$ is relatively low, along with a reduced environmental impact. Currently, research on the use of $LC^3$ in 3D printing applications is relatively limited. However, its advantages in terms of cost and performance present a great potential worthy of further exploration.

Overall, the information outlined in this review has demonstrated that amongst all the alternative binders, geopolymers/alkali-activated systems, MgO-based binders, and $LC^3$ present the highest potential for being used in the development of 3D printed construction components. The widespread application of these alternative binders in the construction industry are dependent on the recognition of their performance characteristics by the building standards on a global scale. The development of other alternative binders could be enhanced via the recognition of their unique capabilities in specific conditions where *PC*-based systems experience shortfalls. This will not only enable the advancement of technical knowledge associated with these alternative binder systems, but also facilitate the development of sustainable 3D printed cementitious components that can be used in a range of construction applications.

## Declaration of competing interest

The authors declare that they have no known competing financial interests or personal relationships that could have appeared to influence the work reported in this paper.

## Data availability

No data was used for the research described in the article.

## Acknowledgement

This work was funded by The Royal Society (project ref: ICA\R1 \201310) and China Scholarship Council (grant number: 202006370082).

## References

[1] Lu B, Weng Y, Li M, Qian Y, Leong KF, Tan MJ, et al. A systematical review of 3D printable cementitious materials. Construct Build Mater 2019;207:477–90.
[2] Wangler T, Roussel N, Bos FP, Salet TAM, Flatt RJ. Digital concrete: a review, vol. 123. Cem Concr Res.; 2019.
[3] Perrot A, Pierre A, Nerella VN, Wolfs RJM, Keita E, Nair SAO, et al. From analytical methods to numerical simulations: a process engineering toolbox for 3D concrete printing. Cem Concr Compos 2021;122:104164.
[4] Siddika A, Mamun MAA, Ferdous W, Saha AK, Alyousef R. 3D-printed concrete: applications, performance, and challenges. J Sustain Cem-Based Mater. 2020;9 (3):127–64.
[5] Ponnamma D, Yin Y, Salim N, Parameswaranpillai J, Thomas S, Hameed N. Recent progress and multifunctional applications of 3D printed graphene nanocomposites. Compos B Eng 2021;204:108493.
[6] Buswell RA, Leal de Silva WR, Jones SZ, Dirrenberger J. 3D printing using concrete extrusion: a roadmap for research. Cement Concr Res 2018;112:37–49.
[7] Yu K, McGee W, Ng TY, Zhu H, Li VC. 3D-printable engineered cementitious composites (3DP-ECC): fresh and hardened properties. Cement Concr Res 2021: 143.
[8] Kalender M, Kılıç SE, Ersoy S, Bozkurt Y, Salman S. Additive manufacturing and 3D printer technology in aerospace industry. In: 2019 9th international conference on recent advances in space technologies (RAST): ieee; 2019. p. 689–94.
[9] Dabbagh SR, Sarabi MR, Rahbarghazi R, Sokullu E, Yetisen AK, Tasoglu S. 3D-Printed microneedles in biomedical applications. iScience; 2020. 102012.
[10] MacDonald E, Wicker R. Multiprocess 3D printing for increasing component functionality. Science 2016;353(6307).
[11] Lewis JA. Direct ink writing of 3D functional materials. Adv Funct Mater 2006;16 (17):2193–204.
[12] Guo C, Zhang M, Bhandari B. Model building and slicing in food 3D printing processes: a review. Compr Rev Food Sci Food Saf 2019;18(4):1052–69.
[13] Tay YWD, Panda B, Paul SC, Noor Mohamed NA, Tan MJ, Leong KF. 3D printing trends in building and construction industry: a review. Virtual Phys Prototyp 2017;12(3):261–76.
[14] Paul SC, Tay YWD, Panda B, Tan MJ. Fresh and hardened properties of 3D printable cementitious materials for building and construction. Arch Civ Mech Eng 2018;18:311–9.
[15] Mechtcherine V, Nerella VN, Will F, Näther M, Otto J, Krause M. Large-scale digital concrete construction – CONPrint3D concept for on-site, monolithic 3D-printing. Autom ConStruct 2019;107.
[16] Zhang X, Flood I, Zhang Y, Moud HI, Hatami M. A cost model to evaluate the economic performance of contour crafting. Computing in civil engineering 2019: visualization, information modeling, and simulation. VA: American Society of Civil Engineers Reston; 2019. p. 618–25.
[17] Kazemian A, Yuan X, Cochran E, Khoshnevis B. Cementitious materials for construction-scale 3D printing: laboratory testing of fresh printing mixture. Construct Build Mater 2017;145:639–47.
[18] Salet T, Wolfs R. Potentials and challenges in 3D concrete printing. In: Proceedings of the 2nd international conference on progress in additive manufacturing; 2016. p. 8–13.
[19] Le TT, Austin SA, Lim S, Buswell RA, Law R, Gibb AG, et al. Hardened properties of high-performance printing concrete. Cement Concr Res 2012;42(3):558–66.
[20] Perkins I, Skitmore M. Three-dimensional printing in the construction industry: a review. Int J Constr Manag 2015;15(1):1–9.
[21] Cesaretti G, Dini E, De Kestelier X, Colla V, Pambaguian L. Building components for an outpost on the Lunar soil by means of a novel 3D printing technology. Acta Astronaut 2014;93:430–50.
[22] Hamidi F, Aslani F. Additive manufacturing of cementitious composites: materials, methods, potentials, and challenges. Construct Build Mater 2019;218: 582–609.
[23] Yu S, Xia M, Sanjayan J, Yang L, Xiao J, Du H. Microstructural characterization of 3D printed concrete. J Build Eng 2021;44:102948.
[24] Voney V, Odaglia P, Brumaud C, Dillenburger B, Habert G. From casting to 3D printing geopolymers: a proof of concept. Cement Concr Res 2021;143:106374.
[25] Khalil A, Wang X, Celik K. 3D printable magnesium oxide concrete: towards sustainable modern architecture. Addit Manuf 2020;33.
[26] Zhang C, Hou Z, Chen C, Zhang Y, Mechtcherine V, Sun Z. Design of 3D printable concrete based on the relationship between flowability of cement paste and optimum aggregate content. Cem Concr Compos 2019;104.
[27] Ye J, Cui C, Yu J, Yu K, Xiao J. Fresh and anisotropic-mechanical properties of 3D printable ultra-high ductile concrete with crumb rubber. Compos B Eng 2021; 211:108639.
[28] Navarrete I, Kurama Y, Escalona N, Lopez M. Impact of physical and physicochemical properties of supplementary cementitious materials on structural build-up of cement-based pastes. Cement Concr Res 2020;130:105994.
[29] Reinold J, Nerella VN, Mechtcherine V, Meschke G. Extrusion process simulation and layer shape prediction during 3D-concrete-printing using the Particle Finite Element Method. 2020.
[30] De Schutter G, Lesage K, Mechtcherine V, Nerella VN, Habert G, Agusti-Juan I. Vision of 3D printing with concrete — technical, economic and environmental potentials. Cement Concr Res 2018;112:25–36.
[31] Ranjbar N, Mehrali M, Kuenzel C, Gundlach C, Pedersen DB, Dolatshahi-Pirouz A, et al. Rheological characterization of 3D printable geopolymers. Cement Concr Res 2021;147:106498.
[32] Chen M, Li L, Wang J, Huang Y, Wang S, Zhao P, et al. Rheological parameters and building time of 3D printing sulphoaluminate cement paste modified by retarder and diatomite. Construct Build Mater 2020:234.
[33] Qian Y, De Schutter G. Enhancing thixotropy of fresh cement pastes with nanoclay in presence of polycarboxylate ether superplasticizer (PCE). Cement Concr Res 2018;111:15–22.
[34] Zhang C, Nerella VN, Krishna A, Wang S, Zhang Y, Mechtcherine V, et al. Mix design concepts for 3D printable concrete: a review. Cem Concr Compos 2021: 104155.
[35] Jiao D, De Schryver R, Shi C, De Schutter G. Thixotropic structural build-up of cement-based materials: a state-of-the-art review. Cem Concr Compos 2021: 104152.
[36] Xu Y, Yuan Q, Li Z, Shi C, Wu Q, Huang Y. Correlation of interlayer properties and rheological behaviors of 3DPC with various printing time intervals. Addit Manuf 2021;47:102327.
[37] Liu C, Chen Y, Xiong Y, Jia L, Ma L, Wang X, et al. Influence of HPMC and SF on buildability of 3D printing foam concrete: from water state and flocculation point of view. Compos B Eng 2022;242:110075.
[38] Perrot A, Rangeard D, Pierre A. Structural built-up of cement-based materials used for 3D-printing extrusion techniques. Mater Struct 2015;49(4):1213–20.
[39] Sikora P, Chougan M, Cuevas K, et al. The effects of nano- and micro-sized additives on 3D printable cementitious and alkali-activated composites: a review. Appl Nanosci 2022;12:805–23. https://doi.org/10.1007/s13204-021-01738-2.
[40] Nerella VN, Hempel S, Mechtcherine V. Effects of layer-interface properties on mechanical performance of concrete elements produced by extrusion-based 3D-printing. Construct Build Mater 2019;205:586–601.
[41] Ramakrishnan S, Muthukrishnan S, Sanjayan J, Pasupathy K. Concrete 3D printing of lightweight elements using hollow-core extrusion of filaments. Cem Concr Compos 2021:104220.
[42] Moelich GM, Kruger J, Combrinck R. Plastic shrinkage cracking in 3D printed concrete. Compos B Eng 2020;200:108313.
[43] Schneider M, Romer M, Tschudin M, Bolio H. Sustainable cement production—present and future. Cement Concr Res 2011;41(7):642–50.

[44] Stafford FN, Dias AC, Arroja L, Labrincha JA, Hotza D. Life cycle assessment of the production of Portland cement: a Southern Europe case study. J Clean Prod 2016;126:159–65.
[45] Shen W, Liu Y, Yan B, Wang J, He P, Zhou C, et al. Cement industry of China: driving force, environment impact and sustainable development. Renew Sustain Energy Rev 2017;75:618–28.
[46] Her S, Park T, Zalnezhad E, Bae S. Synthesis and characterization of cement clinker using recycled pulverized oyster and scallop shell as limestone substitutes. J Clean Prod 2021:278.
[47] Poudyal L, Adhikari K. Environmental sustainability in cement industry: an integrated approach for green and economical cement production. Resour Environ Sustain 2021;4:100024.
[48] Shen W, Cao L, Li Q, Zhang W, Wang G, Li C. Quantifying CO2 emissions from China's cement industry. Renew Sustain Energy Rev 2015;50:1004–12.
[49] Kuzmenko K, Ducoulombier N, Feraille A, Roussel N. Environmental impact of extrusion-based additive manufacturing: generic model, power measurements and influence of printing resolution. Cement Concr Res 2022;157:106807.
[50] Friedlingstein P, O'Sullivan M, Jones MW, Andrew RM, Hauck J, Olsen A, et al. Global carbon budget 2020. Earth Syst Sci Data 2020;12(4):3269–340.
[51] Andrew RM. Global CO 2 emissions from cement production. Earth Syst Sci Data 2018;10(1):195–217.
[52] Tarighat A, Afzali Naniz O. Evaluation of mechanical properties and durability indices of concrete containing wollastonite and silica-fume. J Civ Environ Eng 2017;47(86):47–57.
[53] Thomas BS. Green concrete partially comprised of rice husk ash as a supplementary cementitious material–A comprehensive review. Renew Sustain Energy Rev 2018;82:3913–23.
[54] Kim T, Tae S, Roh S. Assessment of the CO2 emission and cost reduction performance of a low-carbon-emission concrete mix design using an optimal mix design system. Renew Sustain Energy Rev 2013;25:729–41.
[55] Gartner E, Sui T. Alternative cement clinkers. Cement Concr Res 2018;114:27–39.
[56] Duxson P, Fernández-Jiménez A, Provis JL, Lukey GC, Palomo A, van Deventer JS. Geopolymer technology: the current state of the art. J Mater Sci 2007;42(9):2917–33.
[57] Singh B, Ishwarya G, Gupta M, Bhattacharyya SK. Geopolymer concrete: a review of some recent developments. Construct Build Mater 2015;85:78–90.
[58] Palomo A, Grutzeck M, Blanco M. Alkali-activated fly ashes: a cement for the future. Cement Concr Res 1999;29(8):1323–9.
[59] Scrivener KL, Cabiron J-L, Letourneux R. High-performance concretes from calcium aluminate cements. Cement Concr Res 1999;29(8):1215–23.
[60] Winnefeld F, Lothenbach B. Hydration of calcium sulfoaluminate cements—experimental findings and thermodynamic modelling. Cement Concr Res 2010;40(8):1239–47.
[61] Unluer C. Carbon dioxide sequestration in magnesium-based binders. Carbon Dioxide Sequestration in Cementitious Construction Materials 2018:129–73.
[62] Dung NT, Unluer C. Development of MgO concrete with enhanced hydration and carbonation mechanisms. Cement Concr Res 2018;103:160–9.
[63] Mo L, Panesar DK. Effects of accelerated carbonation on the microstructure of Portland cement pastes containing reactive MgO. Cement Concr Res 2012;42(6):769–77.
[64] Arikan M, Sobolev K. The optimization of a gypsum-based composite material. Cement Concr Res 2002;32(11):1725–8.
[65] Yu Q, Brouwers H. Development of a self-compacting gypsum-based lightweight composite. Cem Concr Compos 2012;34(9):1033–43.
[66] Scrivener K, Martirena F, Bishnoi S, Maity S. Calcined clay limestone cements (LC3). Cement Concr Res 2018;114:49–56.
[67] Avet F, Scrivener K. Investigation of the calcined kaolinite content on the hydration of limestone calcined clay cement (LC3). Cement Concr Res 2018;107:124–35.
[68] Berriel SS, Favier A, Domínguez ER, Machado IS, Heierli U, Scrivener K, et al. Assessing the environmental and economic potential of limestone calcined clay cement in Cuba. J Clean Prod 2016;124:361–9.
[69] Ruan S, Unluer C. Comparative life cycle assessment of reactive MgO and Portland cement production. J Clean Prod 2016;137:258–73.
[70] Robayo-Salazar R, Mejía-Arcila J, de Gutiérrez RM, Martínez E. Life cycle assessment (LCA) of an alkali-activated binary concrete based on natural volcanic pozzolan: a comparative analysis to OPC concrete. Construct Build Mater 2018;176:103–11.
[71] Santana HA, Amorim Júnior NS, Ribeiro DV, Cilla MS, Dias CMR. 3D printed mesh reinforced geopolymer: notched prism bending. Cem Concr Compos 2021:116.
[72] Li N, Farzadnia N, Shi C. Microstructural changes in alkali-activated slag mortars induced by accelerated carbonation. Cement Concr Res 2017;100:214–26.
[73] Li N, Shi C, Zhang Z, Zhu D, Hwang H-J, Zhu Y, et al. A mixture proportioning method for the development of performance-based alkali-activated slag-based concrete. Cem Concr Compos 2018;93:163–74.
[74] Roy DM, Jiang W, Silsbee M. Chloride diffusion in ordinary, blended, and alkali-activated cement pastes and its relation to other properties. Cement Concr Res 2000;30(12):1879–84.
[75] Shi C, Stegemann J. Acid corrosion resistance of different cementing materials. Cement Concr Res 2000;30(5):803–8.
[76] Juenger MCG, Winnefeld F, Provis JL, Ideker JH. Advances in alternative cementitious binders. Cement Concr Res 2011;41(12):1232–43.
[77] Komljenović M, Baščarević Z, Bradić V. Mechanical and microstructural properties of alkali-activated fly ash geopolymers. J Hazard Mater 2010;181(1–3):35–42.
[78] Davidovits J. Geopolymer, green chemistry and sustainable development solutions: proceedings of the world congress geopolymer 2005. Geopolymer Institute; 2005.
[79] Li N, Shi C, Zhang Z, Wang H, Liu Y. A review on mixture design methods for geopolymer concrete. Compos B Eng 2019;178:107490.
[80] Yin B, Kang T, Kang J, Chen Y. Analysis of active ion-leaching behavior and the reaction mechanism during alkali activation of low-calcium fly ash. Int J Concr Struct Mater 2018;12(1):1–13.
[81] Yao X, Zhang Z, Zhu H, Chen Y. Geopolymerization process of alkali–metakaolinite characterized by isothermal calorimetry. Thermochim Acta 2009;493(1–2):49–54.
[82] Provis J, Van Deventer J. Geopolymerisation kinetics. 2. Reaction kinetic modelling. Chem Eng Sci 2007;62(9):2318–29.
[83] Yao Y, Hu M, Di Maio F, Cucurachi S. Life cycle assessment of 3D printing geopolymer concrete: an ex-ante study. J Ind Ecol 2019;24(1):116–27.
[84] Ma S, Yang H, Zhao S, He P, Zhang Z, Duan X, et al. 3D-printing of architectured short carbon fiber-geopolymer composite. Compos B Eng 2021;226:109348.
[85] Zhang D-W, Wang D-m, Lin X-Q, Zhang T. The study of the structure rebuilding and yield stress of 3D printing geopolymer pastes. Construct Build Mater 2018;184:575–80.
[86] Panda B, Tan MJ. Experimental study on mix proportion and fresh properties of fly ash based geopolymer for 3D concrete printing. Ceram Int 2018;44(9):10258–65.
[87] Panda B, Unluer C, Tan MJ. Extrusion and rheology characterization of geopolymer nanocomposites used in 3D printing. Compos B Eng 2019;176.
[88] Alghamdi H, Nair SAO, Neithalath N. Insights into material design, extrusion rheology, and properties of 3D-printable alkali-activated fly ash-based binders. Mater Des 2019:167.
[89] Ishwarya G, Singh B, Deshwal S, Bhattacharyya S. Effect of sodium carbonate/sodium silicate activator on the rheology, geopolymerization and strength of fly ash/slag geopolymer pastes. Cem Concr Compos 2019;97:226–38.
[90] Chen Y, Liu C, Cao R, Chen C, Mechtcherine V, Zhang Y. Systematical investigation of rheological performance regarding 3D printing process for alkali-activated materials: effect of precursor nature. Cem Concr Compos 2022;128:104450.
[91] Panda B, Unluer C, Tan MJ. Investigation of the rheology and strength of geopolymer mixtures for extrusion-based 3D printing. Cem Concr Compos 2018;94:307–14.
[92] Panda B, Ruan S, Unluer C, Tan MJ. Investigation of the properties of alkali-activated slag mixes involving the use of nanoclay and nucleation seeds for 3D printing. Compos B Eng 2020:186.
[93] Sun C, Xiang J, Xu M, He Y, Tong Z, Cui X. 3D extrusion free forming of geopolymer composites: materials modification and processing optimization. J Clean Prod 2020;258.
[94] Bong SH, Nematollahi B, Nazari A, Xia M, Sanjayan JG. Fresh and hardened properties of 3D printable geopolymer cured in ambient temperature. First RILEM International Conference on Concrete and Digital Fabrication – Digital Concrete; 2018. p. 3–11. 2019.
[95] Singh NB, Saxena SK, Kumar M, Rai S. Geopolymer cement: synthesis, characterization, properties and applications. Mater Today Proc 2019;15:364–70.
[96] Panda B, Singh GVPB, Unluer C, Tan MJ. Synthesis and characterization of one-part geopolymers for extrusion based 3D concrete printing. J Clean Prod 2019;220:610–9.
[97] Bong SH, Nematollahi B, Nazari A, Xia M, Sanjayan J. Method of optimisation for ambient temperature cured sustainable geopolymers for 3D printing construction applications. Materials 2019;12(6).
[98] Lu C, Zhang Z, Shi C, Li N, Jiao D, Yuan Q. Rheology of alkali-activated materials: a review. Cem Concr Compos 2021;121:104061.
[99] Chougan M, Hamidreza Ghaffar S, Jahanzat M, Albar A, Mujaddedi N, Swash R. The influence of nano-additives in strengthening mechanical performance of 3D printed multi-binder geopolymer composites. Construct Build Mater 2020:250.
[100] Chen Y, Jia L, Liu C, Zhang Z, Ma L, Chen C, et al. Mechanical anisotropy evolution of 3D-printed alkali-activated materials with different GGBFS/FA combinations. J Build Eng 2022;50:104126.
[101] Luukkonen T, Abdollahnejad Z, Yliniemi J, Kinnunen P, Illikainen M. One-part alkali-activated materials: a review. Cement Concr Res 2018;103:21–34.
[102] Xia M, Nematollahi B, Sanjayan J. Printability, accuracy and strength of geopolymer made using powder-based 3D printing for construction applications. Autom ConStruct 2019;101:179–89.
[103] Li Z, Wang L, Ma G, Sanjayan J, Feng D. Strength and ductility enhancement of 3D printing structure reinforced by embedding continuous micro-cables. Construct Build Mater 2020:264.
[104] Lim JH, Panda B, Pham Q-C. Improving flexural characteristics of 3D printed geopolymer composites with in-process steel cable reinforcement. Construct Build Mater 2018;178:32–41.
[105] Li Z, Wang L, Ma G. Mechanical improvement of continuous steel microcable reinforced geopolymer composites for 3D printing subjected to different loading conditions. Compos B Eng 2020:187.
[106] Ma G, Li Z, Wang L, Bai G. Micro-cable reinforced geopolymer composite for extrusion-based 3D printing. Mater Lett 2019;235:144–7.
[107] Korniejenko K, Lach M, Chou SY, Lin WT, Cheng A, Hebdowska-Krupa M, et al. Mechanical properties of short fiber-reinforced geopolymers made by casted and 3D printing methods: a comparative study. Materials 2020;13(3).
[108] Panda B, Paul SC, Mohamed NAN, Tay YWD, Tan MJ. Measurement of tensile bond strength of 3D printed geopolymer mortar. Measurement 2018;113:108–16.

[109] Al-Qutaifi S, Nazari A, Bagheri A. Mechanical properties of layered geopolymer structures applicable in concrete 3D-printing. Construct Build Mater 2018;176:690–9.
[110] Arunothayan AR, Nematollahi B, Ranade R, Bong SH, Sanjayan J. Development of 3D-printable ultra-high performance fiber-reinforced concrete for digital construction. Construct Build Mater 2020;257:119546.
[111] Guo X, Yang J, Xiong G. Influence of supplementary cementitious materials on rheological properties of 3D printed fly ash based geopolymer. Cem Concr Compos 2020;114.
[112] Walling SA, Provis JL. Magnesia-based cements: a journey of 150 Years, and cements for the future? Chem Rev 2016;116(7):4170–204.
[113] Dong HL, Yang EH, Unluer C, Jin F, Al-Tabbaa A. Investigation of the properties of MgO recovered from reject brine obtained from desalination plants. J Clean Prod 2018;196:100–8.
[114] Hay R, Celik K. Hydration, carbonation, strength development and corrosion resistance of reactive MgO cement-based composites. Cement Concr Res 2020;128.
[115] Unluer C, Al-Tabbaa A. The role of brucite, ground granulated blastfurnace slag, and magnesium silicates in the carbonation and performance of MgO cements. Construct Build Mater 2015;94:629–43.
[116] Jin F, Al-Tabbaa A. Characterisation of different commercial reactive magnesia. Adv Cement Res 2014;26(2):101–13.
[117] Huang L, Yang Z, Wang S. Influence of calcination temperature on the structure and hydration of MgO. Construct Build Mater 2020:262.
[118] Thomas JJ, Musso S, Prestini I. Kinetics and activation energy of magnesium oxide hydration. J Am Ceram Soc 2014;97(1):275–82.
[119] Mo LW, Deng M, Tang MS, Al-Tabbaa A. MgO expansive cement and concrete in China: past, present and future. Cement Concr Res 2014;57:1–12.
[120] Silva WM, Aneziris CG, Brito MAM. Effect of alumina and silica on the hydration behavior of magnesia-based refractory castables. J Am Ceram Soc 2011;94(12):4218–25.
[121] Al-Tabbaa A. Reactive magnesia cement. Eco-Efficient Concrete 2013:523–43.
[122] Rocha SD, Mansur MB, Ciminelli VS. Kinetics and mechanistic analysis of caustic magnesia hydration. J Chem Technol Biotechnol: International Research in Process, Environmental & Clean Technology 2004;79(8):816–21.
[123] Dung NT, Hay R, Lesimple A, Celik K, Unluer C. Influence of CO2 concentration on the performance of MgO cement mixes. Cem Concr Compos 2021:115.
[124] Wang L, Chen L, Provis JL, Tsang DCW, Poon CS. Accelerated carbonation of reactive MgO and Portland cement blends under flowing CO2 gas. Cem Concr Compos 2020;106.
[125] Xiao X, Goh LX, Unluer C, Yang E-H. Bacteria-induced internal carbonation of reactive magnesia cement. Construct Build Mater 2021:267.
[126] Ma S, Akca AH, Esposito D, Kawashima S. Influence of aqueous carbonate species on hydration and carbonation of reactive MgO cement. J CO2 Util 2020:41.
[127] Hay R, Celik K. Accelerated carbonation of reactive magnesium oxide cement (RMC)-based composite with supercritical carbon dioxide (scCO2). J Clean Prod 2020:248.
[128] Sinka M, Van den Heede P, De Belie N, Bajare D, Sahmenko G, Korjakins A. Comparative life cycle assessment of magnesium binders as an alternative for hemp concrete. Resour Conserv Recycl 2018;133:288–99.
[129] Park C, Noh M, Park T. Rheological properties of cementitious materials containing mineral admixtures. Cement Concr Res 2005;35(5):842–9.
[130] Kashani A, San Nicolas R, Qiao GG, van Deventer Jsj, Provis JL. Modelling the yield stress of ternary cement–slag–fly ash pastes based on particle size distribution. Powder Technol 2014;266:203–9.
[131] Yuan Q, Zhou D, Li B, Huang H, Shi C. Effect of mineral admixtures on the structural build-up of cement paste. Construct Build Mater 2018;160:117–26.
[132] Abdel-Gawwad HA, Hassan HS, Vásquez-García SR, Israde-Alcántara I, Ding Y-C, Martinez-Cinco MA, et al. Towards a clean environment: the potential application of eco-friendly magnesia-silicate cement in CO2 sequestration. J Clean Prod 2020:252.
[133] Kumar S, Lei J, Yang E-H, Unluer C. Influence of different additives on the rheology and microstructural development of MgO–SiO2 mixes. Compos B Eng 2022;235:109784.
[134] Li ZH, Xu YD, Zhang TS, Hu J, Wei J, Yu Q. Effect of MgO calcination temperature on the reaction products and kinetics of MgO-SiO2-H2O system. J Am Ceram Soc 2019;102(6):3269–85.
[135] Sonat C, Unluer C. Development of magnesium-silicate-hydrate (M-S-H) cement with rice husk ash. J Clean Prod 2019;211:787–803.
[136] Abdel-Gawwad HA, Abd El-Aleem S, Amer AA, El-Didamony H, Arif MA. Combined impact of silicate-amorphicity and MgO-reactivity on the performance of Mg-silicate cement. Construct Build Mater 2018;189:78–85.
[137] Sonat C, Teo WW, Unluer C. Performance and microstructure of MgO-SiO2 concrete under different environments. Construct Build Mater 2018;184:549–64.
[138] Igami Y, Tsuchiyama A, Yamazaki T, Matsumoto M, Kimura Y. In-situ water-immersion experiments on amorphous silicates in the MgO–SiO2 system: implications for the onset of aqueous alteration in primitive meteorites. Geochem Cosmochim Acta 2021;293:86–102.
[139] Sonat C, Dung N, Unluer C. Performance and microstructural development of MgO–SiO2 binders under different curing conditions. Construct Build Mater 2017;154:945–55.
[140] Sonat C, Unluer C. Investigation of the performance and thermal decomposition of MgO and MgO-SiO2 formulations. Thermochim Acta 2017;655:251–61.
[141] Panda B, Sonat C, Yang E-H, Tan MJ, Unluer C. Use of magnesium-silicate-hydrate (M-S-H) cement mixes in 3D printing applications. Cem Concr Compos 2021;117.
[142] Zhang R, Panesar DK. Carbonated binder systems containing reactive MgO and Portland cement: strength, chemical composition and pore structure. J Clean Prod 2020:271.
[143] Zhang R. Carbonated reactive MgO–Portland cement blends: chemistry, microstructure and properties. 2018.
[144] Haque MA, Chen B. Research progresses on magnesium phosphate cement: a review. Construct Build Mater 2019;211:885–98.
[145] Fan S, Chen B. Experimental study of phosphate salts influencing properties of magnesium phosphate cement. Construct Build Mater 2014;65:480–6.
[146] Lahalle H, Coumes CCD, Mesbah A, Lambertin D, Cannes C, Delpech S, et al. Investigation of magnesium phosphate cement hydration in diluted suspension and its retardation by boric acid. Cement Concr Res 2016;87:77–86.
[147] Viani A, Gualtieri AF. Preparation of magnesium phosphate cement by recycling the product of thermal transformation of asbestos containing wastes. Cement Concr Res 2014;58:56–66.
[148] Joon Woo Park, Ki Hwan Kim, Ki Yong Ann. Fundamental Properties of Magnesium Phosphate Cement Mortar for Rapid Repair of Concrete. Advances in Materials Science and Engineering 2016; 2016;7179403:7. https://doi.org/10.1155/2016/7179403.
[149] Li Y, Chen B. Factors that affect the properties of magnesium phosphate cement. Construct Build Mater 2013;47:977–83.
[150] Zhang Y, Wang S, Zhang B, Hou D, Li H, Li L, et al. A preliminary investigation of the properties of potassium magnesium phosphate cement-based grouts mixed with fly ash, water glass and bentonite. Construct Build Mater 2020;237.
[151] Li DX, Feng CH. Study on modification of the magnesium phosphate cement-based material by fly ash. Adv Mater Res 2010;150–151:1655–61.
[152] Wang HT, Cao JH, Xue M, Li SM. Effect of phosphate cement and aggregate on the fluidity and strength of phosphate concrete. Adv Mater Res 2010;168–170:1859–63.
[153] Zhao S, Yan H, Zhang H, Wang H, Li Y, Hu Z, et al. The effects of admixtures of inorganic hydrates on the hydration hardening of magnesium potassium phosphate cement. Adv Cement Res 2018;30(2):83–92.
[154] Weng Y, Ruan S, Li M, Mo L, Unluer C, Tan MJ, et al. Feasibility study on sustainable magnesium potassium phosphate cement paste for 3D printing. Construct Build Mater 2019;221:595–603.
[155] Zhao Z, Chen M, Xu J, Li L, Huang Y, Yang L, et al. Mix design and rheological properties of magnesium potassium phosphate cement composites based on the 3D printing extrusion system. Construct Build Mater 2021;284:122797.
[156] Zhao Z, Chen M, Jin Y, Lu L, Li L. Rheology control towards 3D printed magnesium potassium phosphate cement composites. Compos B Eng 2022:109963.
[157] Fu YC, Cao XP, Li ZJ. Printability of magnesium potassium phosphate cement with different mixing proportion for repairing concrete structures in severe environment. Key Eng Mater: Trans Tech Publ; 2016. p. 989–95.
[158] Deng D. The mechanism for soluble phosphates to improve the water resistance of magnesium oxychloride cement. Cement Concr Res 2003;33(9):1311–7.
[159] Wu C, Yu H, Zhang H, Dong J, Wen J, Tan Y. Effects of phosphoric acid and phosphates on magnesium oxysulfate cement. Mater Struct 2015;48(4):907–17.
[160] Li K, Wang Y, Yao N, Zhang A. Recent progress of magnesium oxychloride cement: manufacture, curing, structure and performance. Construct Build Mater 2020;255.
[161] Huang T, Yu C, Yuan Q, Liu Z, Deng D. Effect of alcohol leachable chloride on strength of magnesium oxychloride cement. J Am Ceram Soc 2020;103(10):5927–38.
[162] Xiang L, Liu F, Li J, Jin Y. Hydrothermal formation and characterization of magnesium oxysulfate whiskers. Mater Chem Phys 2004;87(2–3):424–9.
[163] Barbieri V, Gualtieri ML, Manfredini T, Siligardi C. Hydration kinetics and microstructural development of a magnesium oxysulfate cement modified by macromolecules. Construct Build Mater 2020;248:118624.
[164] Sinka M, Zorica J, Bajare D, Sahmenko G, Korjakins A. Fast setting binders for application in 3D printing of bio-based building materials. Sustainability 2020;12(21).
[165] Wu J, Chen H, Guan B, Xia Y, Sheng Y, Fang J. Effect of fly ash on rheological properties of magnesium oxychloride cement. J Mater Civ Eng 2019;31(3).
[166] Wu J, Guan B, Chen H, Tian H, Liu J, Xiong R. Effects of polycarboxylate superplasticiser on the early hydration properties of magnesium oxychloride cement. Construct Build Mater 2020;259.
[167] Chen C, Wu C, Zhang H, Chen Y, Niu J, Chen F, et al. Effect of superplasticisers and their mechanisms of action on magnesium oxysulfate cement properties. Adv Cement Res 2020;32(5):225–33.
[168] Şengül K, Erdoğan ST. Influence of ground perlite on the hydration and strength development of calcium aluminate cement mortars. Construct Build Mater 2021:266.
[169] Scrivener K, Capmas A. Calcium aluminate cements. Adv Concr Technol 2003:1–31.
[170] Fan W, Zhuge Y, Ma X, Chow CWK, Gorjian N. Strain hardening behaviour of PE fibre reinforced calcium aluminate cement (CAC) – ground granulated blast furnace (GGBFS) blended mortar. Construct Build Mater 2020:241.
[171] Qi C, Spagnoli D, Fourie A. Structural, electronic, and mechanical properties of calcium aluminate cements: insight from first-principles theory. Construct Build Mater 2020;264.
[172] Maier A-K, Dezmirean L, Will J, Greil P. Three-dimensional printing of flash-setting calcium aluminate cement. J Mater Sci 2010;46(9):2947–54.
[173] Shakor P, Sanjayan J, Nazari A, Nejadi S. Modified 3D printed powder to cement-based material and mechanical properties of cement scaffold used in 3D printing. Construct Build Mater 2017;138:398–409.

[174] Huang T, Li B, Yuan Q, Shi Z, Xie Y, Shi C. Rheological behavior of Portland clinker-calcium sulphoaluminate clinker-anhydrite ternary blend. Cem Concr Compos 2019;104.
[175] Tan H, Guo Y, Zou F, Jian S, Ma B, Zhi Z. Effect of borax on rheology of calcium sulphoaluminate cement paste in the presence of polycarboxylate superplasticizer. Construct Build Mater 2017;139:277–85.
[176] Guo X, Shi H, Hu W, Wu K. Durability and microstructure of CSA cement-based materials from MSWI fly ash. Cem Concr Compos 2014;46:26–31.
[177] Liu C, Xiong Y, Chen Y, Jia L, Ma L, Deng Z, et al. Effect of sulphoaluminate cement on fresh and hardened properties of 3D printing foamed concrete. Compos B Eng 2022;232:109619.
[178] Chen M, Yang L, Zheng Y, Huang Y, Li L, Zhao P, et al. Yield stress and thixotropy control of 3D-printed calcium sulfoaluminate cement composites with metakaolin related to structural build-up. Construct Build Mater 2020:252.
[179] Ingaglio J, Fox J, Naito CJ, Bocchini P. Material characteristics of binder jet 3D printed hydrated CSA cement with the addition of fine aggregates. Construct Build Mater 2019;206:494–503.
[180] Ding Z, Wang X, Sanjayan J, Zou PXW, Ding ZK. A feasibility study on HPMC-improved sulphoaluminate cement for 3D printing. Materials 2018;11(12).
[181] Chen M, Li L, Zheng Y, Zhao P, Lu L, Cheng X. Rheological and mechanical properties of admixtures modified 3D printing sulphoaluminate cementitious materials. Construct Build Mater 2018;189:601–11.
[182] Shahzad Q, Wang X, Wang W, Wan Y, Li G, Ren C, et al. Coordinated adjustment and optimization of setting time, flowability, and mechanical strength for construction 3D printing material derived from solid waste. Construct Build Mater 2020;259.
[183] Chen M, Guo X, Zheng Y, Li L, Yan Z, Zhao P, et al. Effect of tartaric acid on the printable, rheological and mechanical properties of 3D printing sulphoaluminate cement paste. Materials 2018;11(12).
[184] Khalil N, Aouad G, El Cheikh K, Rémond S. Use of calcium sulfoaluminate cements for setting control of 3D-printing mortars. Construct Build Mater 2017;157:382–91.
[185] Ma G, Salman NM, Wang L, Wang F. A novel additive mortar leveraging internal curing for enhancing interlayer bonding of cementitious composite for 3D printing. Construct Build Mater 2020;244.
[186] Liu C, Gao J, Tang Y, Chen X. Preparation and characterization of gypsum-based materials used for 3D robocasting. J Mater Sci 2018;53(24):16415–22.
[187] Santos T, Gomes MI, Silva AS, Ferraz E, Faria P. Comparison of mineralogical, mechanical and hygroscopic characteristic of earthen, gypsum and cement-based plasters. Construct Build Mater 2020;254:119222.
[188] Raii M, Escudero Sanz FJ, Nzihou A. Rheological behavior of gypsum, plaster, and hydroxyapatite gel blends. Ind Eng Chem Res 2012;51(34):11163–9.
[189] Feng Q, Deng Y, Kim H, Lei W, Sun Z, Jia Y, et al. Observation and analysis of gypsum particleboard using SEM. J Wuhan Univ Technol -Materials Sci Ed 2007;22(1):44–7.
[190] Ma B, Jiang Q, Huang J, Wang X, Leng J. Effect of different silica particles on flowability of gypsum powder for 3D powder printing. Construct Build Mater 2019;217:394–402.
[191] Peng J, Qu J, Zhang J, Chen M, Wan T. Adsorption characteristics of water-reducing agents on gypsum surface and its effect on the rheology of gypsum plaster. Cement Concr Res 2005;35(3):527–31.
[192] Zhi Z, Ma B, Tan H, Guo Y, Jin Z, Yu H, et al. Effect of competitive adsorption between polycarboxylate superplasticizer and hydroxypropylmethyl cellulose on rheology of gypsum paste. J Mater Civ Eng 2018;30(7).
[193] Feng P, Meng X, Chen J-F, Ye L. Mechanical properties of structures 3D printed with cementitious powders. Construct Build Mater 2015;93:486–97.
[194] Kong L, Ostadhassan M, Li C, Tamimi N. Can 3-D printed gypsum samples replicate natural rocks? An experimental study. Rock Mech Rock Eng 2018;51(10):3061–74.
[195] Kong L, Ostadhassan M, Li C, Tamimi N. Pore characterization of 3D-printed gypsum rocks: a comprehensive approach. J Mater Sci 2018;53(7):5063–78.
[196] Kong L, Ostadhassan M, Lin R, Li C. Nanoscale mechanical properties of 3D printed gypsum-powder-based rocks by nanoindentation and numerical modeling. Rapid Prototyp J 2019;25(7):1295–308.
[197] Aslan R, Turan O. Gypsum-based sound absorber produced by 3D printing technology. Appl Acoust 2020:161.
[198] Danner T, Norden G, Justnes H. Characterisation of calcined raw clays suitable as supplementary cementitious materials. Appl Clay Sci 2018;162:391–402.
[199] Scrivener K, Favier A. Calcined clays for sustainable concrete. Springer; 2015.
[200] Chen Y, Romero Rodriguez C, Li Z, Chen B, Çopuroğlu O, Schlangen E. Effect of different grade levels of calcined clays on fresh and hardened properties of ternary-blended cementitious materials for 3D printing. Cem Concr Compos 2020;114.
[201] Chen Li, Chaves F, Çopuroğlu Veer, Schlangen. Limestone and calcined clay-based sustainable cementitious materials for 3D concrete printing: a fundamental study of extrudability and early-age strength development. Appl Sci 2019;9(9).
[202] Chen Y, Chaves Figueiredo S, Li Z, Chang Z, Jansen K, Çopuroğlu O, et al. Improving printability of limestone-calcined clay-based cementitious materials by using viscosity-modifying admixture. Cement Concr Res 2020:132.
[203] Chen Y, He S, Zhang Y, Wan Z, Çopuroğlu O, Schlangen E. 3D printing of calcined clay-limestone-based cementitious materials. Cement Concr Res 2021;149:106553.
[204] Chen Y, Chaves Figueiredo S, Yalcinkaya C, Copuroglu O, Veer F, Schlangen E. The effect of viscosity-modifying admixture on the extrudability of limestone and calcined clay-based cementitious material for extrusion-based 3D concrete printing. Materials 2019;12(9).
[205] Chen Y, Jansen K, Zhang H, Romero Rodriguez C, Gan Y, Çopuroğlu O, et al. Effect of printing parameters on interlayer bond strength of 3D printed limestone-calcined clay-based cementitious materials: an experimental and numerical study. Construct Build Mater 2020:262.
[206] Atzeni C, Pia G, Sanna U, Spanu N. Surface wear resistance of chemically or thermally stabilized earth-based materials. Mater Struct 2008;41(4):751–8.
[207] Perrot A, Rangeard D, Courteille E. 3D printing of earth-based materials: processing aspects. Construct Build Mater 2018;172:670–6.
[208] Dubois V, Leblanc A, Carpentier O, Alhaik G, Wirquin E. Performances of flax shive-based lightweight composites with rapid hardening. Construct Build Mater 2018;165:17–27.
[209] Thomas BS, Damare A, Gupta R. Strength and durability characteristics of copper tailing concrete. Construct Build Mater 2013;48:894–900.
[210] Zhao S, Fan J, Sun W. Utilization of iron ore tailings as fine aggregate in ultra-high performance concrete. Construct Build Mater 2014;50:540–8.
[211] Li X, Zhang N, Yuan J, Wang X, Zhang Y, Chen F, et al. Preparation and microstructural characterization of a novel 3D printable building material composed of copper tailings and iron tailings. Construct Build Mater 2020;249.
[212] Panda B, Ruan S, Unluer C, Tan MJ. Improving the 3D printability of high volume fly ash mixtures via the use of nano attapulgite clay. Compos B Eng 2019;165:75–83.
[213] Panda B, Tan MJ. Rheological behavior of high volume fly ash mixtures containing micro silica for digital construction application. Mater Lett 2019;237:348–51.
[214] Duan Z, Hou S, Xiao J, Singh A. Rheological properties of mortar containing recycled powders from construction and demolition wastes. Construct Build Mater 2020;237:117622.
[215] Hou S, Xiao J, Duan Z, Ma G. Fresh properties of 3D printed mortar with recycled powder. Construct Build Mater 2021;309:125186.
[216] Liu Y, Shi C, Yuan Q, An X, Jiao D, Zhu L, et al. An amendment of rotation speed-torque transformation equation for the Herschel-Bulkley model in wide-gap coaxial cylinders rheometer. Construct Build Mater 2020;237:117530.
[217] Liu Y, Shi C, Yuan Q, An X, Zhu L, Wu B. The rotation speed-torque transformation equation of the Robertson-Stiff model in wide gap coaxial cylinders rheometer and its applications for fresh concrete. Cem Concr Compos 2020;107:103511.
[218] Heirman G, Vandewalle L, Van Gemert D, Wallevik O. Integration approach of the Couette inverse problem of powder type self-compacting concrete in a wide-gap concentric cylinder rheometer. J Non-Newtonian Fluid Mech 2008;150(2–3):93–103.
[219] Feys D, Wallevik JE, Yahia A, Khayat KH, Wallevik OH. Extension of the Reiner–Riwlin equation to determine modified Bingham parameters measured in coaxial cylinders rheometers. Mater Struct 2013;46(1):289–311.
[220] Bullard JW, Jennings HM, Livingston RA, Nonat A, Scherer GW, Schweitzer JS, et al. Mechanisms of cement hydration. Cement Concr Res 2011;41(12):1208–23.
[221] Frías M, Cabrera J. Pore size distribution and degree of hydration of metakaolin–cement pastes. Cement Concr Res 2000;30(4):561–9.
[222] Cahn JW. The kinetics of grain boundary nucleated reactions. Acta Metall 1956;4(5):449–59.
[223] Krstulović R, Dabić P. A conceptual model of the cement hydration process. Cement Concr Res 2000;30(5):693–8.
[224] Van Riessen A. Thermo-mechanical and microstructural characterisation of sodium-poly (sialate-siloxo)(Na-PSS) geopolymers. J Mater Sci 2007;42(9):3117–23.
[225] Baščarević Z, Komljenović M, Miladinović Z, Nikolić V, Marjanović N, Petrović R. Impact of sodium sulfate solution on mechanical properties and structure of fly ash based geopolymers. Mater Struct 2015;48(3):683–97.
[226] Lin T, Jia D, Wang M, He P, Liang D. Effects of fibre content on mechanical properties and fracture behaviour of short carbon fibre reinforced geopolymer matrix composites. Bull Mater Sci 2009;32(1):77–81.
[227] Neto AAM, Cincotto MA, Repette W. Drying and autogenous shrinkage of pastes and mortars with activated slag cement. Cement Concr Res 2008;38(4):565–74.
[228] Chen M, Liu B, Li L, Cao L, Huang Y, Wang S, et al. Rheological parameters, thixotropy and creep of 3D-printed calcium sulfoaluminate cement composites modified by bentonite. Compos B Eng 2020;186:107821.
[229] Hou P, Muzenda TR, Li Q, Chen H, Kawashima S, Sui T, et al. Mechanisms dominating thixotropy in limestone calcined clay cement (LC3). Cement Concr Res 2021;140:106316.
[230] Mohammad M, Masad E, Al-Ghamdi SG. 3D concrete printing sustainability: a comparative life cycle assessment of four construction method scenarios. Buildings 2020;10(12):245.
[231] Abdalla H, Fattah KP, Abdallah M, Tamimi AK. Environmental footprint and economics of a full-scale 3D-printed house. Sustainability 2021;13(21):11978.
[232] Gosselin C, Duballet R, Roux P, Gaudillière N, Dirrenberger J, Morel P. Large-scale 3D printing of ultra-high performance concrete–a new processing route for architects and builders. Mater Des 2016;100:102–9.
[233] Bos FP, Menna C, Pradena M, Kreiger E, da Silva WL, Rehman AU, et al. The realities of additively manufactured concrete structures in practice. Cement Concr Res 2022;156:106746.
[234] Pessoa S, Guimarães A, Lucas S, Simões N. 3D printing in the construction industry-A systematic review of the thermal performance in buildings. Renew Sustain Energy Rev 2021;141:110794.
[235] Xiao J, Ji G, Zhang Y, Ma G, Mechtcherine V, Pan J, et al. Large-scale 3D printing concrete technology: current status and future opportunities. Cem Concr Compos 2021:104115.

[236] Bai G, Wang L, Ma G, Sanjayan J, Bai M. 3D printing eco-friendly concrete containing under-utilised and waste solids as aggregates. Cem Concr Compos 2021;120:104037.
[237] Bong SH, Xia M, Nematollahi B, Shi C. Ambient temperature cured 'just-add-water'geopolymer for 3D concrete printing applications. Cem Concr Compos 2021;121:104060.
[238] Zhou G-X, Li C, Zhao Z, Qi Y-Z, Yang Z-H, Jia D-C, et al. 3D printing geopolymer nanocomposites: graphene oxide size effects on a reactive matrix. Carbon 2020; 164:215–23.
[239] Korniejenko K, Łach M, Chou S, Lin W, Mikuła J, Mierzwiński D, et al. A comparative study of mechanical properties of fly ash-based geopolymer made by casted and 3D Printing methods. In: IOP conference series: materials science and engineering: IOP publishing; 2019, 012005.
[240] Panda B, Paul SC, Hui LJ, Tay YWD, Tan MJ. Additive manufacturing of geopolymer for sustainable built environment. J Clean Prod 2017;167:281–8.
[241] Xia M, Sanjayan J. Method of formulating geopolymer for 3D printing for construction applications. Mater Des 2016;110:382–90.
[242] Xia M, Sanjayan JG. Methods of enhancing strength of geopolymer produced from powder-based 3D printing process. Mater Lett 2018;227:281–3.
[243] Nematollahi B, Xia M, Sanjayan J. Post-processing methods to improve strength of particle-bed 3D printed geopolymer for digital construction applications. Front Mater 2019;6.
[244] Panda B, Noor Mohamed NA, Tay YWD, Tan MJ. Bond strength in 3D printed geopolymer mortar. In: First RILEM international conference on concrete and digital fabrication – digital concrete; 2019. p. 200–6. 2018.
[245] Wang L, Ma G, Liu T, Buswell R, Li Z. Interlayer reinforcement of 3D printed concrete by the in-process deposition of U-nails. Cement Concr Res 2021;148: 106535.